2016

Comparisons of Ablator Experimental Performance to Response Modeling and Effects of Water Phase Transition in Porous TPS Materials

David L. Smith
University of Kentucky, davidleosmith145@gmail.com
Digital Object Identifier: https://doi.org/10.13023/ETD.2016.501

Recommended Citation

Smith, David L., "Comparisons of Ablator Experimental Performance to Response Modeling and Effects of Water Phase Transition in Porous TPS Materials" (2016). *Theses and Dissertations--Mechanical Engineering*. 83.
https://uknowledge.uky.edu/me_etds/83

STUDENT AGREEMENT:

I represent that my thesis or dissertation and abstract are my original work. Proper attribution has been given to all outside sources. I understand that I am solely responsible for obtaining any needed copyright permissions. I have obtained needed written permission statement(s) from the owner(s) of each third-party copyrighted matter to be included in my work, allowing electronic distribution (if such use is not permitted by the fair use doctrine) which will be submitted to UKnowledge as Additional File.

I hereby grant to The University of Kentucky and its agents the irrevocable, non-exclusive, and royalty-free license to archive and make accessible my work in whole or in part in all forms of media, now or hereafter known. I agree that the document mentioned above may be made available immediately for worldwide access unless an embargo applies.

I retain all other ownership rights to the copyright of my work. I also retain the right to use in future works (such as articles or books) all or part of my work. I understand that I am free to register the copyright to my work.

REVIEW, APPROVAL AND ACCEPTANCE

The document mentioned above has been reviewed and accepted by the student's advisor, on behalf of the advisory committee, and by the Director of Graduate Studies (DGS), on behalf of the program; we verify that this is the final, approved version of the student's thesis including all changes required by the advisory committee. The undersigned agree to abide by the statements above.

David L. Smith, Student

Dr. Alexandre Martin, Major Professor

Dr. Haluk E. Karaca, Director of Graduate Studies

Comparisons of ablator experimental performance to response modeling and effects of water phase transition in porous TPS materials

---

THESIS

A thesis submitted in partial
fulfillment of the requirements for
the degree of Master of Science in
Mechanical Engineering in the
College of Engineering at the
University of Kentucky

By
David L. Smith
Lexington, Kentucky

Director: Dr. Alexandre Martin, Ph.D., P.E., Associate Professor of Mechanical Engineering
Lexington, Kentucky 2016

ABSTRACT OF THESIS

Comparisons of ablator experimental performance to response modeling and effects of water phase transition in porous TPS materials

The Mars Science Laboratory Entry Descent and Landing Instrumentation (MEDLI) project performed extensive arc jet tests for development, qualification, and calibration of instrumented heat shield plugs. These plugs each contained several thermocouples for recording near-surface and in-depth temperature response of the Phenolic Impregnated Carbon Ablator (PICA) heat shield. The arc jet test results are entered into a comprehensive database so that broad trends across the test series can be compared. One method of analysis is to compare with ablator material response calculations and solve the in-depth heat conduction equations. Using the near-surface thermocouple measurements as a boundary condition in numerical simulations, comparisons are made with other thermocouple measurements taken deeper within the TPS test article. The work presented here uses this technique to compare test results with model simulations using several metrics, such as peak-temperature difference, maximum difference in temperature, and a total integrated temperature deviation. A significant difference in prediction behavior with respect to the location of source thermocouple is shown based on these comparisons. The temperature prediction accuracy is quantified for the tested material and material response code and is found to be highly dependent on the distance between the boundary condition thermocouple and the deeper reference thermocouple. Based on this test data, it is shown that numerical models can predict in-depth temperature measurements equally well for sensor plugs installed in the arc jet test model with or without a silicone adhesive. It is found that predicted temperatures are consistently greater than measured values, indicating the PICA material model is generally conservative for in-depth temperature predictions. In addition, a low-temperature phenomenon was consistently observed through thermocouple measurements deep within the material during the MEDLI arc jet testing. This anomaly, referred to here as the “hump,” consists of a change in concavity of the temperature profile well below the maximum temperature and is seen in various TPS materials and atmospheric conditions, and typically occurs around 40 °C. It is proposed that the observed “hump” is a result of the heat of vaporization during the endothermic phase transition of water within the TPS material. This is supported by the known absorption of water by PICA from the atmosphere prior to testing or flight. The presented material response model captures energy effects of phase transition from a pre-existing water presence. This work shows that water presence currently appears to be the most probable cause for the phenomenon, which is observed in multiple different porous TPS materials.

KEYWORDS: atmospheric entry, thermal protection system, material response, numerical heat transfer, arc jet testing, experimental modeling

Author's signature: David L. Smith

Date: December 5, 2016

Comparisons of ablator experimental performance to response modeling and effects of water phase transition in porous TPS materials

By
David L. Smith

Director of Thesis: Alexandre Martin, Ph.D., P.E.

Director of Graduate Studies: Haluk E. Karaca, Ph.D.

Date: December 5, 2016

Dedicated to my wife, Lauren Michelle Smith,
for her loving support and motivation.

ACKNOWLEDGMENTS

My most sincere thanks goes to Dr. Alexandre Martin for serving as my research advisor and for giving me the opportunity to join the Gas Surface Interaction Lab to pursue my Master's degree. Dr. Martin's counsel in both my graduate and undergraduate studies as an academic mentor has been inspiring, and my work would not be possible without his guidance, motivation, patience, and superb technical expertise in ablation modeling field.

I would like to extend my thanks to Dr. José Graña-Otero and Dr. Kaveh A. Tagavi at University of Kentucky for serving on my thesis advisory committee. Special thanks also goes to my fellow researchers: Dr. H. Weng, A. Omidy, R. Davuluri, J. Cooper, Dr. H. Zhang, and the remaining members of the Gas Surface Interaction research group at the University of Kentucky, for their technical contributions, support, encouragement, and friendship.

I would also like to thank Mr. Todd White at ERC, Inc. for serving as a mentor throughout my studies. I am also thankful for Dr. David Hash and his summer research program at NASA Ames Research Center. Special thanks to the MEDLI project team member and NASA arc jet facilities team for their experimental results. Specifically, I would like to thank J. Santos and M. Olson, principal investigators of the MEDLI test series, for their help and cooperation during the database construction portion of this work and M. Mahzari for contributions to the FIAT analysis methods.

Financial support for this work was provided by the MEDLI project and NASA Kentucky EPSCoR Award NNX13AN04A. Research assistantships provided by Department of Mechanical Engineering at University of Kentucky.

TABLE OF CONTENTS

LIST OF FIGURES

LIST OF TABLES

Nomenclature

Scalars

A	surface area of a control volume, m^2
A_i	pre-exponential factor of solid component i, s^{-1}
A_w	reaction rate coefficient, s^{-1}
E_i/R	activation energy of solid component i over universal gas constant, K
E_g	overall gas energy per unit volume, J/m^3 or kg/ms^2
E_s	overall solid energy per unit volume, J/m^3 or kg/ms^2
E_w	overall water energy per unit volume, J/m^3 or kg/ms^2
h	gas enthalpy, J/kg
λ	thermal conductivity, W/mK
λ_s	solid material thermal conductivity, W/mK
λ_{w_l}	liquid water thermal conductivity, W/mK
N	Number of samples
p	static pressure, Pa
p_w	sample surface pressure, Pa
q_w	sample surface heat flux, W/m^2
t	time, s
T	temperature, K
T_{sat}	saturation temperature, K
V_w	volume occupied by water, m^3
V	volume of a control volume, m^3
Γ_i	volume fraction of virgin solid composite i
Δ	discretized term
ω_{s_i}	decomposition rate of solid component i, kg/m^{3}s
ω_{w_i}	decomposition rate of water component i, kg/m^{3}s

ϕ	porosity of material
ψ_i	phenomenological parameter for component i
ρ_g	overall density of pyrolysis gases, kg/m^3
ρ_s	overall solid density, kg/m^3
ρ_{s_i}	density of solid component i, kg/m^3
ρ_{w_i}	density of water component i, kg/m^3
ω	reaction rate of gas/solid/water species, kg/m^{3}s
ξ_i	effective density of water component i, kg/m^3

Vectors

$\mathbf{D}$	diffusive source terms in momentum equations, Pa/m
$\mathbf{F}_{cond}$	conductive heat flux, $(F_{cond,x}, F_{cond,y}, F_{cond,z})$, W/m^2
$\mathbf{n}$	face normal direction
$\mathbf{P}$	vector of primitive variables
$\mathbf{Q}$	vector of conservative variables
$\mathbf{RHS}$	right hand side of the linear system to be solved
$\mathbf{S}$	vector of source terms in a control volume
$\mathbf{u}$	velocity components (u,v,w) of Cartesian coordinates, m/s

Matrices

$\boldsymbol{\mathcal{F}}$	convective flux through the face of a control volume
$\boldsymbol{\mathcal{F}}_d$	diffusive flux through the face of a control volume

Subscripts

F	FIAT

g	overall pyrolysis gas
M	measured
i	time index of the sample
l	liquid state of water
s	solid
v	vapor state of water
w	water component
x, y, z	components of Cartesian coordinate system

Chapter 1 Introduction

1.1 Background

Thermal protection systems (TPS) are utilized to protect vehicles from aerodynamic heating during atmospheric entry. For extreme heating conditions, ablative materials are employed to limit heat transfer. They ensure vehicle safety by reducing heat flux through various phenomena such as oxidation, pyrolysis chemical reactions, and generated gas blowing effects [10–12]. Light-weight ablative materials are commonly made of a fibrous non-pyrolyzing matrix impregnated with a phenolic pyrolyzing resin. As the temperature of the phenolic increases, endothermic reactions absorb heat and produce gases that are expelled from the TPS with cooling effects (see Figure 1.1). Modeling of these effects is performed through Material Response (MR) codes [13–17] which can, in turn, be coupled with Computational Fluid Dynamics (CFD) [18–21] codes. This can be used to obtain accurate heating characteristics and to optimize the TPS thickness for specific mission requirements and flight profiles. Accuracy of material response modeling is an important aspect of vehicle design since the TPS accounts for a significant portion of the weight of entry spacecraft, and inadequate heat protection can severely damage vehicles, or even lead to mission failure. Optimal design thickness is a function of the ablative material behavior, and thus, its capacity to keep the payload at safe temperatures.

On August 6, 2012, the Mars Science Laboratory Spacecraft (MSL) entry spacecraft landed the Curiosity rover, the largest ever interplanetary payload to date, in the Gale Crater on Mars [22]. MSL's surface was tiled 4.5 meter diameter heat shield constructed from an ablative material called Phenolic Impregnated Carbon Ablator (PICA) [23] which protected the vehicle from the excessive heat experienced dur-

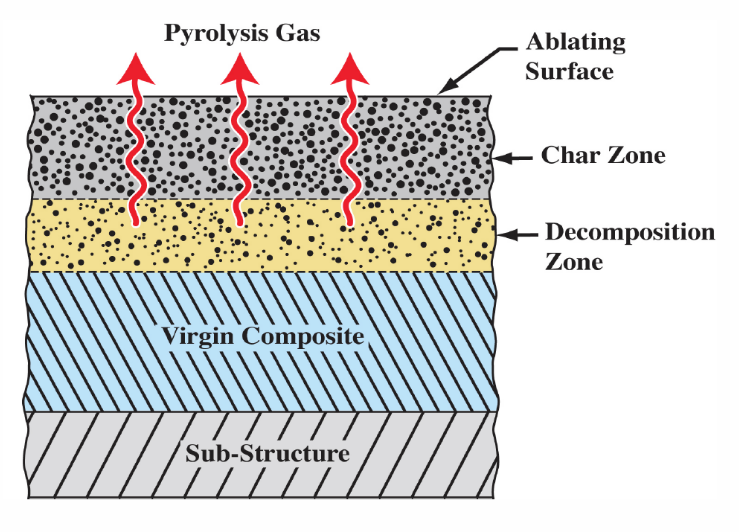

Figure 1.1: Schematic of a decomposing ablator zones and product gas [1].

ing entry from interplanetary trajectories. An artistic rendering of the MSL entry is shown in Figure 1.2. The heat shield incorporated the MSL Entry, Descent, and Landing Instrumentation (MEDLI) suite, which consisted of two main components: MEDLI Integrated Sensor Plugs (MISP) and Mars Entry Atmospheric Data System (MEADS) [3]. The MEDLI system was designed to capture entry data associated with the heat shield performance and heating conditions. Each MISP unit contained embedded, temperature-recording thermocouples and a Hollow aErothermal Ablation and Temperature (HEAT) sensor [24]. The HEAT sensors were designed to track in-depth material response characteristics, such as the char region, and the the to record the data. The MISP unites each contained multiple thermocouples, and thus, each MISP provided several time-varying temperature measurements of the ablative material's response to the aerothermal environment. The heat shield served its purpose and successfully protected the precious payload from the high convective heat fluxes, and the MEDLI system successfully returned entry temperature, pressure, and recession data from the Martian atmospheric entry to NASA scientists.

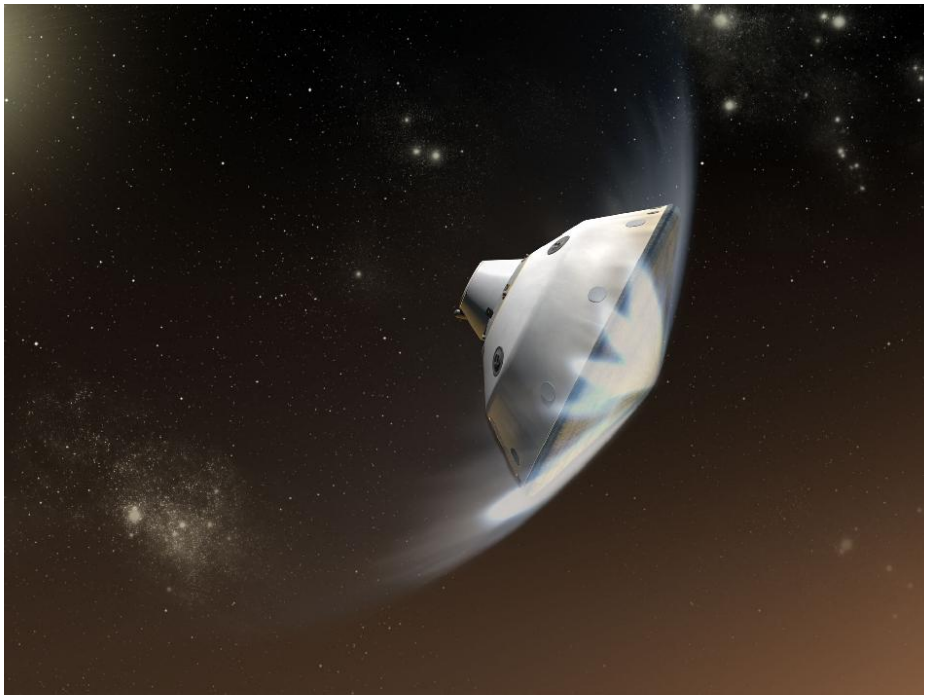

Figure 1.2: Artistic rendering of the MSL spacecraft entering the Martian atmosphere [2].

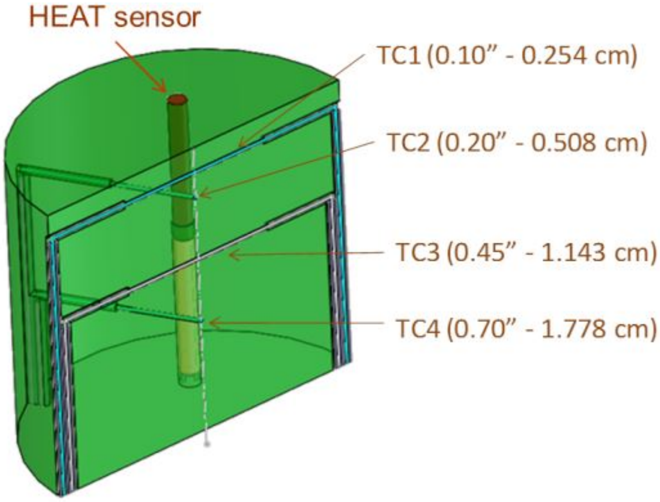

Figure 1.3: Cross Section of MEDLI Integrated Sensor Plug showing nominal thermocouple depths and HEAT sensor. Image from Ref. 3.

1.2 MEDLI system testing and arc jet database

As part of the development and calibration of the MISP plugs, extensive testing was carried out at NASA Ames Research Center in order to qualify the new instrument prior to launch [25–27]. This testing was necessary to ensure that the plugs would not adversely affect the performance of the heat shield. After the MISP was determined to be safe for mission use, additional tests were completed to characterize the thermal response of the sensors. All of these tests are collectively referred to as the MEDLI test campaign. The test articles were constructed with PICA material in various configurations and most would include at least one MISP unit. Tests were conducted in arc jet facilities which force high-temperature, high-enthalpy flow over the surface of the test articles to simulate atmospheric entry conditions. As a result, the temperature of the test article surface would increase and initiate the ablation process, and the internal temperature of the TPS material would increase.

Over the course of the MEDLI test campaign, it was recognized that the vast amount of data obtained could be compiled, analyzed, and used to quantify the fidelity of numerical models. More specifically, the data could provide an opportunity to assess the accuracy of the material model used in the material response codes. The material models used in such codes are complex [11, 12] and account for multiple physical and chemical phenomena such as pyrolysis, decomposition, and surface recession [28]. Current material models are usually built using data from many single-parameter tests to characterize individual material properties [29]. The MEDLI test campaign provides an opportunity to compare material response predictive capabilities over a large data set of similar tests using the same ablative material.

By comparing the result from the MR numerical model to the performance of the test articles in the MEDLI test campaign, a quantitative analysis can be performed. Tests results from the MEDLI suite were collected in an extensive database in which material response predictions could be compared. The database is described in detail in subsequent chapters and its analysis is the focus of this research. This thesis documents the methodology used to build the MEDLI arc jet database and proposes a number of statistical metrics for use in comparing PICA temperature data from arc jets with the numerical model predictions in Chapter 3. The statistical data are summarized and the discrepancies with the numerical, predictive results are highlighted.

1.3 Low-temperature phenomena presence in PICA

Observed during the MEDLI test series and MSL flight data, a low-temperature phenomena within the material was consistently measured by the thermocouples further from the surface [6]. This anomaly consists of a change in concavity of the temperature profile during the heating phase of the material and well before maximum temperature is attained. The anomaly has been given the name "the hump" throughout this work, and it is defined as a local minimum in the temperature derivative. The phenomenon consistently occurs around 40 °C in the MEDLI test data, which can be seen in figures throughout Chapter 4. The low-temperature "hump" is also seen in cases with materials other than PICA [8, 30]. Current MR models fail to predict the temperature profile concavity change which causes overprediction of peak temperatures within the material [6]. The hump temperatures in the MEDLI test series correlate well with the known saturation curve of water. It is proposed in this research work that the observed "hump" is a result of the heat of vaporization during the endothermic phase transition of the water within the TPS material. The endothermic reaction absorbs additional heat from the surroundings, which temporarily reduces the local temperature gradient. This hypothesis is highly supported by the known absorption of water by PICA and other carbon-phenolic porous materials from the atmosphere prior to testing or flight [30]. One goal of the proceeding research is to determine the effects of a liquid to vapor water transition within the porous TPS material.

In Chapter 4, the effects of a liquid-to-vapor water phase transition within the TPS material are explored. Because water phase transition is believed to be the major contributor to this phenomenon, other possible effects of water presence are temporarily neglected in order to simplify the model. Some of these potential factors may include changes in heat capacity, thermal conductivity, and gas phase equilibrium. The low-temperature "hump" phenomenon seen in multiple carbon phenolic ablators is recreated within a material response code by implementing a water phase transition model. The work aims to provide supporting evidence to the hypothesis that water is causing the irregularity seen for in-depth temperature profiles. The work also presents supporting evidence from experimental cases, along with preliminary model results, and explores the nature of these changes, as well as discusses future research that can be completed in this field of study.

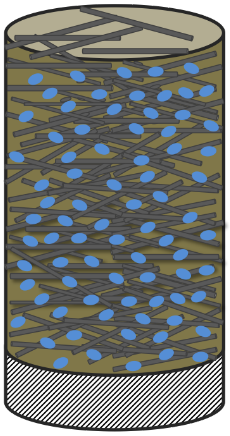

Figure 1.4: Schematic of a decomposing ablator with water

Chapter 2 Literature Review

2.1 Thermal protection system instrumentation and experimental data

Atmospheric entry is one of the most challenging portions of many space missions because aerodynamic heating threatens the payload with extremely high temperatures. In order to protect an entry vehicle, thermal protection systems are used to keep the interior of the spacecraft at safe temperatures. One category of TPS is an ablative material, which reduces the heat flux through various phenomena such as oxidation, pyrolysis chemical reactions, generated gas blowing effects, charring, etc. [10–12]. Ablative materials are effective and reliable for vehicle protection in heating conditions due to the combination of these phenomena. They are used on space vehicles, ballistic-entry vehicles, and various other research vehicles. Ablators are typically lightweight and made up of thermosetting resins such as phenolics, epoxies, and silicones and can include a reinforcement structure composed of carbon graphite or other materials. Selection of TPS construction material is based on the entry profile parameters like heat flux, pressure gradients, vehicle geometry, and entry flight time. Like any TPS material, ablative materials come with the cost of added weight to the spacecraft, and because launching additional payload is a costly endeavor, optimizing heat shield design is of particular interest to the space exploration community. In addition, advancements in TPS technology allow for safe Entry, Descent, and Landing (EDL) during missions which strive to challenge the boundaries of space exploration and align with increasingly challenging flight profiles. To do so, an in-depth understanding of the physical response of the thermal system is necessary. Scientists look to experimental data in the form of both flight and ground testing, as well as simulation results, for atmospheric entry modeling (explored in Section 2.2), in order to advance scientific understanding or entry phenomena and to push the boundaries of space exploration.

Various techniques have been used to capture experimental TPS data including embedded instrumentation, in-test spectral observation, and post-test inspections. Since sending a vehicle into space is a costly endeavor, less expensive ground-based experiments provide an excellent TPS testing outlet. Flight-based experiments typically evolve as secondary missions which hitch rides with primary space exploration initiatives, such as Mars Pathfinder, Stardust Sample Return, and Mars Science Laboratory.

Flight testing and observations

Apollo 4 and Apollo 6 missions were two of the first major instrumented heat shield test flights. As unmanned missions, the mission objective was to demonstrate the capability of the ablative heat shield at lunar return velocities. The Apollo command module heat shield was made of AVCOAT material consisting of an expoxy novolac resin within a fiberglass honeycomb matrix. Temperatures were measured with in-depth thermocouple plugs, also made of AVCOAT [31]. These thermocouples were positioned at strategic depths and different locations around the capsule shell to measure and understand the aerothermal environment. These measurements were compared with results from pre-flight predicted temperature data and simulations in order to build confidence in the analytical methods for in-depth temperature predictions for lunar-return entry.

Space Shuttle tiles have also been instrumented with in-depth thermocouples for reasons similar to that of the Apollo experimentation. Shuttle instrumentation has been studied extensively, but its TPS is of a non-ablative style. A recent example of capsule instrumentation is the Orion EFT1 mission, which contained many instruments embedded in AVCOAT plugs [30, 32].

Another instrumented flight example is the Mars Pathfinder mission. Pathfinder successfully returned Martian EDL data when it delivered the first rover on Mars, called Sojourner [33,34]. Mars Pathfinder used SLA-561V, a silicone- and cork-based ablator in a phenolic honeycomb matrix with a series of thermocouples installed beneath the TPS surface to capture "bond line" temperatures during entry. Spencer et al. [33] attempted to recreate the atmosperic entry conditions using the data collected from these thermocouples.

Spectral observation can also be used to collect data from entry vehicles. A prime example of this is the Stardust sample return mission, where the capsule entry was the fastest into Earth's atmosphere of any vehicle. The capsule was observed by multiple optical instruments during reentry to Earth's atmosphere, and the collected data was used to calculate heat flux and surface temperature of the vehicle [35].

In order to continue the advancement of EDL technologies, MSL's heat shield was instrumented with the MEDLI suite. MEDLI was an extensive and important project for the aerothermodynamic community, and MSL's successful entry was a very significant advancement for NASA's EDL capabilities. MSL's heat shield was designed to withstand heating rates greater than 200 W/cm^2 during hypersonic entry, which is of greater value than those for any of the previous Martian entries [3]. In addition, the MEDLI instrumentation suite was more advanced than any other blunt body entry instrumentation mission and provided a plethora of data to further develop technologies within the EDL system [6]. For example, these future technologies consist of larger vehicles, increased entry speeds, or even deployable TPS. With the pressure, temperature, and recession sensors incorporated into the MEADS, MISP, and HEAT units (introduced in Section 1.1), extensive studies have been completed on MSL's entry and on the characteristics of the MEDLI system, including this thesis [4,6,36–39].

In order for the MEDLI entry data to be valuable, the component construction and instrumentation design were meticulously specified. The seven MISP units in MEDLI each included four K-type thermocouples and one HEAT sensor. The MISP were cylindrical plugs: 1.3 inches in diameter and 1.14 inches deep [24]. The thermocouples were located at nominal depths of 0.10, 0.20, 0.45, and 0.70 inches from the surface, as can be seen in Figure 1.3 and were secured using a vulcanized silicone sealant (RTV) between the plug and the bulk PICA tiles [24]. Figure 2.1 shows the locations of the MISP units on the MSL heat shield. Each HEAT sensor consisted of platinum-tungsten wires which were wound around a central Kaplon tube [4]. As an isotherm correlated with the melting point of the platinum-tungsten wires traces through the material, the wires would electrically short and the change in total resistance of the sensor was monitored. This data, in conjunction with the thermocouple data used to correct for thermal effects on the platinum-tungsten resistivity, was intended to track an isotherm though the TPS. However, the resulting HEAT data did not consistently behave as expected, and future work must been completed with the received data for accurate interpretation. The MISP plugs temperature profiles, along with the MEADS surface pressure measurements taken at other strategic locations, proved useful for recreating aerothermodynamic flight conditions.

White et al. [4] go into great detail about where the MISP plugs are strategically located in the MSL heat shield and provide x-ray depths for the thermocouples installed for each MISP location. This information is useful for further analysis of the MEDLI flight data, explored in Section 2.3.

Ground testing

Recreating entry conditions in ground-based testing facilities can be a very effective way to explore the capabilities of thermal protection systems. A common ground-based test is in an arc jet, where enthalpy flow exiting a convergent-divergent nozzle is forced over the surface of the test article to simulate atmospheric entry conditions.

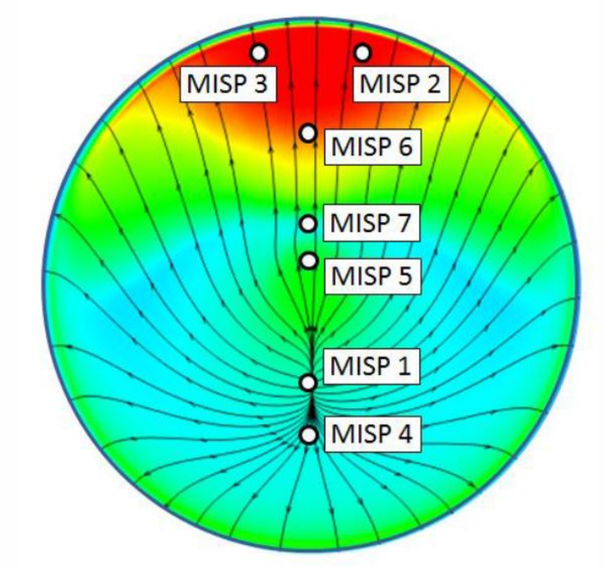

Figure 2.1: Locations of MISP plugs on MSL PICA heat shield surface [4].

Ground-based testing offers many advantages over flight tests such as controllability, repeatably, and most importantly, cost effectiveness. Using arc jet facilities can also be less design-intensive than in-flight experimentation. Arc jet testing is used to develop new TPS configurations and to study existing technology. For example, the instrumented MISP unit went through rigorous testing at various arc jet facilities (particularly at NASA Ames Research Center) in order to become certified for flight on MSL [25–27]. The testing ensured that the plugs would not adversely affect the performance of the heat shield, but also served as an experimental case to study and characterize the thermal response of the PICA material and MEDLI sensors.

2.2 Material Response for TPS modeling

Material Response codes are used to model the behavior of TPS materials during atmospheric entry. They numerically simulate heating conditions to accurately replicate the thermophysical materials' response and serve as a critical component to entry vehicle design. The development of ablation MR codes is studied intensively in research facilities around the world, some of which are introduced and described generally throughout this section. Accuracy of the material response modeling is an important aspect of vehicle design since the TPS accounts for a significant portion of the weight of the spacecraft.

One useful diagram can be seen in Figure 2.2 [5], which explains various types of material response code, and the level of complexity involved with the implementation of each phenomena.

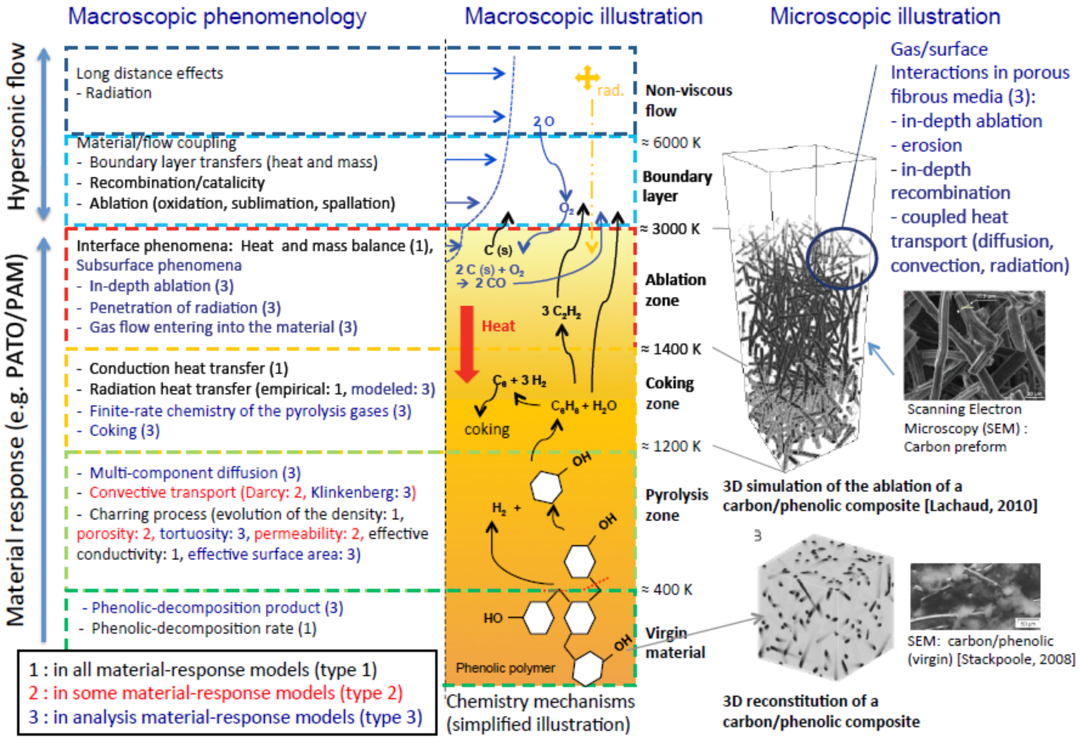

Figure 2.2: Illustration of the phenomenology of porous ablative materials [5]

One example of an MR code for ablation modeling is NASA's Fully Implicit Ablation and Thermal response (FIAT) [17]. FIAT models phenolic decomposition, effective conductivity, and ablation. It is one of the simpler material response codes that has been used for many years in the NASA community, and it used extensively in Chapter 3 of this work.

When developing material response codes, verification and evaluating accuracy by experimental validation are both necessary. Amar [1] shows the verification of a one-dimensional material thermal response code using a finite control volume. Continuity equations are solved using Fourier's law for heat conduction and Darcy's law for porous flow, and implementation of terms are discussed thoroughly. Amar presents the procedure for developing an ablation modeling tool that is consistent with other methods and performs verification studies that will be used when verifying future work. The results of Amar's research code [1] for the carbon-phenolic thermochemical ablation problem are compared with those of other accepted models, and differences are thoroughly discussed. A historical view of material response modeling is presented by Amar, and references can be made for a clear understanding and implementation of various methods. The verification process of the presented ablation code can serve as a reference for future work intended to verify and validate a model presenting an additional energy term.

One major advance of Material Response codes can be their versatility to simulate various physical models. For example, Martin and Boyd [40] discuss the differences seen in using different laws to model the effects of pyrolysis gas within an ablator. This is done in order to accurately improve heat shield ablation rate modeling for entry vehicle thermal protection systems. The two laws of focus are Forchheimer's law and Darcy's law. Forchheimer's law is typically used for very high velocities in a porous media where in inertial effects must be accounted properly. Forchheimer's law behaves similarly to Darcy's law, except with an additional inertial term. The Reynolds number is historically used to decide if the inertial term should be implemented, which presents the issue of determining an appropriate characteristic length for the Reynolds number calculation. When using pore size, various characteristics of porosity is not taken into account such as tortuosity and closed porosity. Using a modified version of Forchheimer's law is proposed, which reduces to Darcy's law when Forchhiemer number (an indicator of when pore size is perceivable at a macroscopic level) is very small [40], and thus, both laws can be accounted for in the same MR code.

Martin and Boyd [40] also show the formulation of the material response code MOPAR. It explains the governing equations: mixture energy equation, solid phase equation, gas-phase continuity equation, and momentum equation in addition to Darcy's and Forchheimer's law. Model validation was preformed to insure that MOPAR behaves as expected by performing nonlinear convergence studies, boundary condition verifications, and timing studies. Other validations are done using code-to-code comparisons with codes from Sandia National Laboratories. Comparison with experimental results was also completed with carbon-phenolic test cases in arc jet flows, which is a primary focus of subsequent chapters of this thesis. The presented comparisons show discrepancies between the measured and computed results and provide various possible explanations for shown discrepancies such as the empirical thermochemical tables not being calculated for the exact material used. Another possible explanation for differences seen in the ablation front measurements could be the lack of thermal expansion in the model. Expansion was observed in the test material, and depending on the reversibility of this process, variations in thickness measurements were possible.

The Porous-martial Analysis Toolbox based on Open FOAM-extend (PATO) is a modular analysis platform implemented to test various physics-based models for porous materials. PATO is governed by the same general conservation equations presented by Amar [1], but it is designed in order to easily study specific aspects of the porous media response to high temperature environments on a global or elementary scale. Lachaud et al. [5] go on to explain the inner working of PATO which, unlike FIAT, solved the momentum equation for pressure along with many other capabilities. The major concept behind PATO is that it is an extremely flexible tool where various model configurations can easily be adapted and implemented. If the hypothesis proposed for the low-temperature "hump" is indeed proved plausible, it is likely that water simulation will be added to the list of phenomena that need to be accounted. PATO could serve as a platform to accommodate these changes for the NASA community.

KATS

In this work, the Kentucky Aerodynamic and Thermal-response System (KATS) developed by A. Martin and Weng et al. is used [7]. KATS MR module can be loosely coupled with a the KATS CFD module. KATS is an implementation of a three-dimensional material response code for charring ablative materials. The pyrolysis gas flow through the material is calculated for with various boundary conditions, such the Iso-Q geometry used in arc jet test facilities. The gas momentum model uses the extension of Darcy's Law discussed by Martin et al. [40].

Weng et al. [7] presents several test cases performed using a theoretical light-weight ablator called TACOT with material properties loosely based on PICA [7] and identical initial boundary conditions. Weng then explains the series of cases with changing directional permeability and thermal conductivity of the model. As expected, the change in these orthotropic material properties affected the pyrolysis gas flow and internal thermal response greatly. Directions with higher permeability have enhanced gas flow, and one result of this effect is the ability to control pyrolysis gas flow in a design setting, because carbon-phenolic is naturally an anisotropic material. Also as expected, the orthotropic thermal conductivity greatly affected the thermal response.

This work shows that it is very important to model orthotropic properties correctly in a material response code. It also shows how relevant a three-dimensional code is to the community because one-dimensional codes would clearly be unable to accurately model an orthotropic material. Similar verification techniques are implemented, and the details described here proved insight into the logistics of using the KATS and the model's governing equations and assumptions. It is also be possible to simulate an arc jet test article using a TC driving technique with the three-dimensional code. This is of particular interest because the one-dimensional assumption is less reasonable for arc jet models than for large entry vehicles.

Material response model validation

Model validation with experimental tests is a key topic explored in this work. One example of an existing example of an experimental validation with a material response code is the Stardust sample return mission introduced in Section 2.1. After the Stardust capsule entry was observed during reentry, the measured heat flux and surface temperature of the vehicle were compared to computational predictions. The CFD solution coupled with a material response code resulted in a predicted heat flux which differed only 1% from the measured heat flux [35]. There was overprediction of surface temperature at altitudes about 75 km, which is believed to be a result of the zinc and potassium emission from an ablating white paint which cools the surface. Also, the experimental data shows that loosely coupled CFD and material response code is a reliable approach to predict entry vehicle surface conditions, including temperature. This is a key advancement in the future of partially and fully coupled CFD and material response codes.

These spectral instruments captured low-light emissions and spectral intensity from the entry vehicle in order to measure vehicle surface temperature during heating. The measurements were then compared with coupled CFD and material response model predictions. The models used overpredicted observed temperatures by less than 50 K in the early stages of the descent. From the spectrometer in Czerny-Turner configuration telescope, analysis agreed within 5% of the average surface temperature from the loosely coupled model including the peak heating period [35]. This was is an impressively high correlation for simulation results and that of a reentry observation experiment.

This subject is directly related to the work presented in this thesis in that it involves comparison of material response models for PICA and measured flight results. Between the Stardust and MSL cases, two comparisons between numerical models and full-trajectory flight exposure are made using PICA material. With the MEDLI test series drawing similar comparisons, the results here are useful and provide an alternative approach to the heating conditions from in-depth thermocouples to those seen the in MEDLI system. The PICA emissivity material properties are discussed along with the coupling capabilities between the DPLR CFD code and the material response code FIAT. These findings are supportive for computational and experimental comparison, similar to those explored later in Section 2.3 and Chapter 3.

2.3 MSL flight and simulation comparisons

After the MEDLI suite (introduced in Section 2.1) successfully measured and transmitted entry data to NASA scientists, the results were compared to material response predictions [3, 4, 36]. The predictions are obtained using a CFD-calculated heating profile and NASA's material response code, FIAT. Figure 2.3 shows the measured flight temperature response along with the predicted temperature profiles at the various thermocouple depths. It can be seen that the estimated heating environment and the material response model shows significant differences with the flight data, namely the maximum obtained temperature for the shallower thermocouples. The prediction models significantly overpredict the maximum measured temperatures as well. Also, an unexpected change in concavity occurred in deeper thermocouple responses, which can be easily observed in MISP 1, 2, 3, 4, and 6, and the modeled results do not predict any change in concavity in this low-temperature regime.

As seen in Figure 2.3, the MISP flight data has many distinct trends. In the top thermocouple (TC1) a significant change in slope of the temperature profile is observed in the 800 K range. This is believed to be the result of turbulent flow

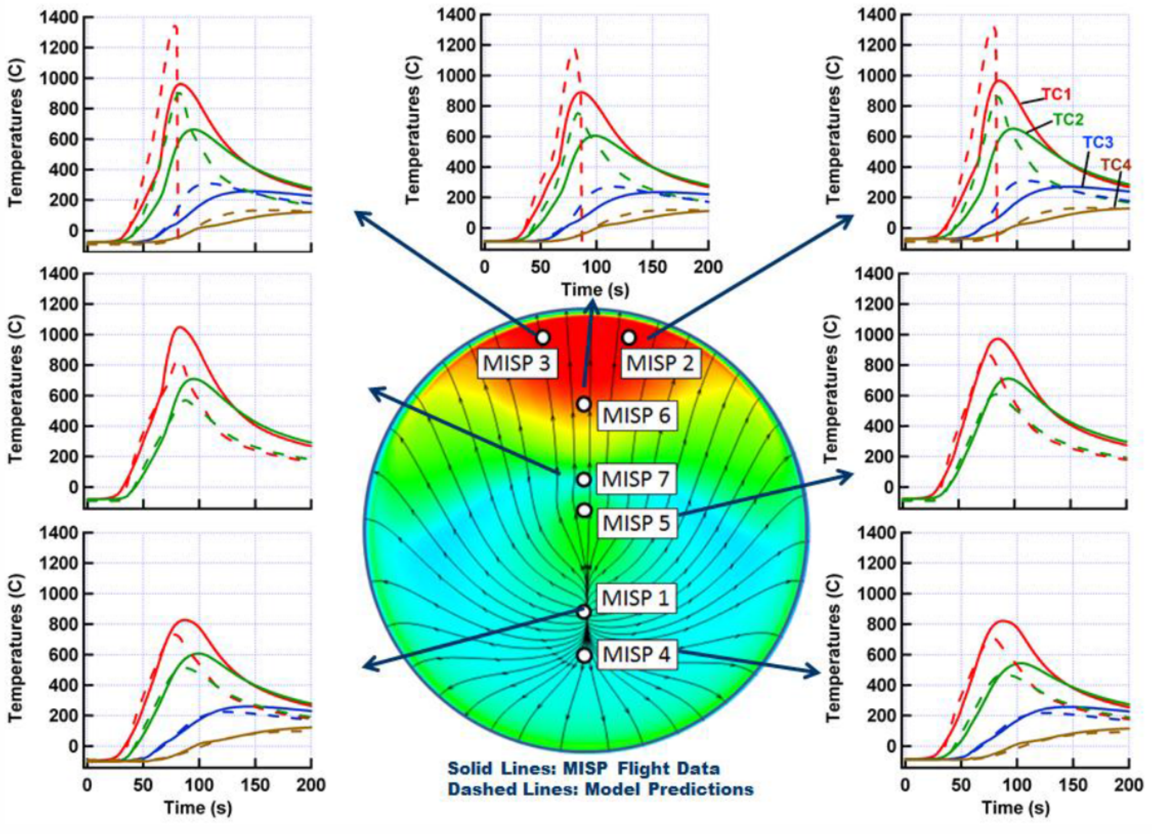

Figure 2.3: MISP flight data with temperature predictions from MSL flight. TC1 is located nearest the ablation surface, and subsequent TC's progress deeper into the material. Image from Ref. [3]

transition [4]. White et al. [4] discusses when turbulent transition was expected for each MISP plug using roughness-induced transition criteria and how PICA arc jet test samples were studied in order to estimate surface roughness. The inferred transition times occurred between two to ten seconds after prediction transitions times for all MISP excluding MISP 1 and MISP 4, which did not see clear transition (with the exception of MISP 7, which experienced transition closer to the desired time). It is also shown that the early transition is likely not caused by PICA gap fillers or the MISP plug variations on the surface of the TPS. Another trend of interest is how the material response model predicts the cooling effects. As seen in Figure 2.3, after peak heating, the thermocouples locations are expected to cool down significantly faster than what is observed. This could be a result of many different phenomena such as uncertainties in the char material properties, lower surface emissivity, or simply higher surface heating than expected [41]. These unknowns are of significant concern because TPS for vehicle design is usually constrained by "bond line" temperature. Also note that the maximum TC1 temperature is overpredicted in the MISPs furthest from the stagnation point (MISP 2, 3, and 6) while the maximum TC1 temperature is under predicted in the other regions. It is believed that this is the case because the turbulent heating was not overpredicted, and as a result, the model predicts that the surface in this region will recess beyond the first thermocouple, and hence why the predicted temperature is not defined for the complete duration of the simulation [4]. Based on these results, it is difficult to access the accuracy of the material properties and MR model due to possible errors at the surface. These errors include the CFD model, flow characteristics, material surface properties, surface recession, and radiation. In order to accurately compare the in-depth material characteristics, a different technique is needed.

Following the initial predictions, Mahzari et al. [37] developed a technique to directly compare MEDLI flight data with the in-depth heat conduction MR simulation, done by using near-surface thermocouple measurements as a boundary condition within a material response code. This is advantageous since surface boundary conditions have a high uncertainty. The analysis technique is called the "TC driver" method. The effects of depth measurement uncertainty on the method accuracy is also studied by Mahzari et al. [37]. Within the MEDLI sensor plugs, the thermocouple depths from the surface of the TPS have a known uncertainty determined by x-ray imaging of the plugs. The work presents the TC driver analysis while looking at upper, nominal, and lower bounds for the thermocouple depths. This is done by shifting the depth of the driving TC up while the remaining depths are offset to the lower possible positions. The result is a lower bound for the temperature predictions. In contrast, an upper bound to the temperature predictions results from the driving thermocouple being offset down and the reference thermocouples being offset up. It is seen in 2.4 that the nominal FIAT solutions overpredict the flight data for the lower TC3 and TC4, and this overprediction is indicative of errors in virgin PICA properties [6, 41]. Mahzari et al. showed the results from TC driving analysis with FIAT MR code and the MEDLI flight data. Similar analysis with FIAT TC driving is completed in Chapter 3 with emphasis on capturing quantitative data to measure the differences between predicted and experimental in-depth temperatures, and applied to the breadth of the MEDLI test series data.

White et al. [4] go into great detail about the TC driver analysis completed with the MISP flight data. As seen in Figure 2.4, the TC driving predictions are fairly accurate with respect to the second thermocouple (TC2) with only slight overprediction while the in-depth thermocouples are not predicted as well for the TC1 driver. Because there are four TCs for each MISP, alternate thermocouples can be used for the boundary condition, and the further in-depth response can evaluated with the remaining thermocouples. For example, TC2 can be used as a boundary condition, and results can be compared with measurements from TC4. One main advantage that this poses is that, for instance, when wanting to only look at virgin material properties, TC3 can be used as a driver for TC4. Another advantage of this technique is that it decouples the surface heating conditions from the conduction modeling. The TC driving method is useful for applying relatively easily obtainable test data to model and material characteristics, and the work presented is a good background on the technique.

The TC driver method does have a shortcoming: it does not simulate conditions at the heating surface. FIAT is built to simulate internal temperatures based on a defined set of boundary conditions, and because the MISP thermocouples measured in-depth temperatures, the TC driver method only simulates conditions between the driving TC and the bond line. Therefore, a method is needed to use the thermocouple

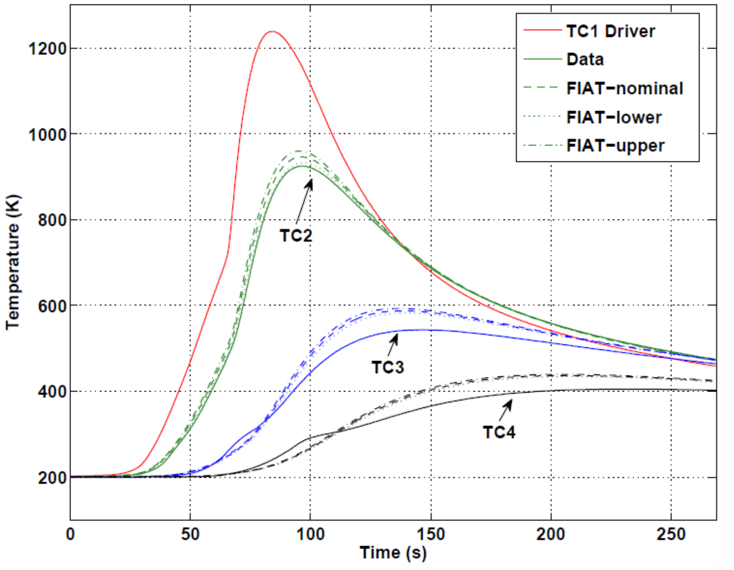

Figure 2.4: Flight MISP 2 thermocouple driver analysis with depth uncertainty [6]

data for surface condition estimation. Mahzari et al. [6] developed and implemented an inverse reconstruction method to do so. The technique modifies the surface conditions and calculates the difference between model predictions and the measured flight data. Then, it makes adjustments to the boundary conditions (at the surface) in order to minimize this quantitative difference. The work completed by Mahzari et al. [6] goes on to explain the details of the inverse analysis method and other sensitivity analysis for the MEDLI flight data case. Mahzari et al. uses the measured temperatures to calculate surface conditions such as heat flux and compare the results with CFD predictions and the various techniques of doing so are discussed.

Low-temperature phenomena

Mahzari et al. also explored the unexpected temperature “hump” (as introduced in Section 1.3) in the deeper thermocouple temperature profiles and noted how it was observed in all of the MISP locations, but did not postulate a possible physical explanation [6]. The existing tools are not able to model the “hump” behavior, and model predictions are not expected to match the data. Seen in Figure 2.4, the “hump” is not accurately predicted using the thermocouple driver approach, and therefore, a strong correlation for these thermocouples in this temperature regime was not necessarily expected when modeling virgin material. Mahzari et al. provide a strong impetus for the “hump” problem to be resolved because the use of in-depth thermocouple data is limited for other applications, such as the uncertainty analysis and bond-line temperature restrictions, until this phenomena is accurately modeled.

Chapter 3 Comparisons of PICA In-depth Material Performance and Ablator Response Modeling from MEDLI Arc Jet Tests

3.1 Overview

Over the course of the MEDLI test campaign, it was recognized that the vast amount of data obtained could be compiled, analyzed, and used to quantify the fidelity of numerical models. More specifically, the data could provide an opportunity to assess the accuracy of the material model used in the Material Response (MR) codes. The work in this chapter documents the methodology used to build the MEDLI arc jet database and proposes a number of statistical metrics for use in comparing PICA temperature data from arc jets with the numerical model predictions. The quantitative techniques used to evaluate the MEDLI test campaign data are similar to those implemented by Mahzari et al. to assess MSL flight data. The statistical data are summarized and the discrepancies with the numerical, predictive results are identified and highlighted.

3.2 The MEDLI arc jet database

In total, the MEDLI test campaign was comprised of eleven test series completed between 2007 and 2014 in four different arc jet facilities and resulted in more than 75 individual test articles [27]. The arc jet facilities provided ground-based hyperthermal environments by using a direct current source to heat test gases and force them through various nozzles, such as a convergent-divergent nozzle. During a test, models were individually inserted into the flow and heated for a specified duration. The test parameters were selected to match expected flight heat flux, pressure, and heat load. Throughout the MEDLI test series, MISPs were tested in many different arc jet flow conditions, which is seen below in Figure 3.1. The plugs were installed into larger PICA models using different techniques such as simply inserting (press-fit) or applying a vulcanized silicone sealant around the plug (RTV bonded). Each test series consisted of multiple instrumented TPS models. The model configuration was either a suspended stagnation article or wedge (testing in the IHF and AHF facilities at NASA Ames Research Center), or a panel (testing in the PTF and TFD facilities at NASA Ames Research Center). Panel TPS models included multiple MISP plugs, while stagnation and wedge configurations contained only one MISP. For stagnation-configured tests, calibration probes were inserted into the flow prior to the test article in order to measure stagnation pressure, heat flux, and flow enthalpy. The model was then inserted by mechanical "sting" arm for the desired test duration. For panel-configured tests, calibration plates were used to make these measurements. Early MISP tests were performed with plugs in the SLA-561V ablator. However, the majority of the test campaign was conducted on the PICA ablator after the MSL project changed to a PICA heat shield design [42].

In order to easily reference the test conditions, model configurations, results, and other metadata, a central database was compiled. Table 3.1 includes a list of parameters included in the MEDLI database.

The compiled database was used as a reference source for the MEDLI testing analysis. An example application of the metadata is illustrated in Figure 3.1 and shows the type of test articles that were used for different testing conditions. It is hoped that the compiled information will be used as reference for future experimental design at NASA Ames Research Center and other arc jet facilities.

After compiling the metadata in Table 3.1 and the data files into a central location and consistent format, an analysis of the MISP thermal response was performed. The

Table 3.1: Metadata for MEDLI arc jet testing database

Test Series Information	Test Conditions	Model Information	Miscellaneous
Facility[1]	Model Time In	Model Geometry	Notes
Date	Model Time Out	Number of MISP	Test Objectives
Principle Investigator	Heating Type[2]	Model Diameter	LN Soak
Model Serial Number	Arc Heater Voltage	Model Material[6]	Post-Test Core
Run Number	Arc Heater Current	Model Serial Number	Last Known Location
Sting Arm	Arc Heater Pressure	Model Drawing Number	Data File Information
Test Date	Main Air Flow	MISP Serial Number	
Test Engineer	Argon Mass Concentration	HEAT Serial Number	
Target Cold-wall Hear Rate	Calorimeter Enthalpy	Raw Plug Serial Number	
Desired Heat Load	Calorimeter Stag. Pressure	Material Billet Number	
Target Pressure	Calorimeter Heat Flux	Installation Method[3]	
Desired Test Duration	Calorimeter Geometry	Recession Measurements	
	Average Surface Temp.[5]	Number of Thermocouples	
	Nozzle Diameter	Thermocouple Type[4]	
		Thermocouple X-ray Depth	
		Material Stack-up	

[1] Aerodynamic Heating Facility, Turbulent Flow Duct, Panel Test Facility, or Interaction Heating Facility

[2] Measured from pyrometer

[3] Press-fit or RTV bonded

[4] Smart or Type-K

[5] Constant or Ramped

[6] Early testing used SLA-561V material, a cork-based ablator in a phenolic honeycomb matrix, instead of PICA.

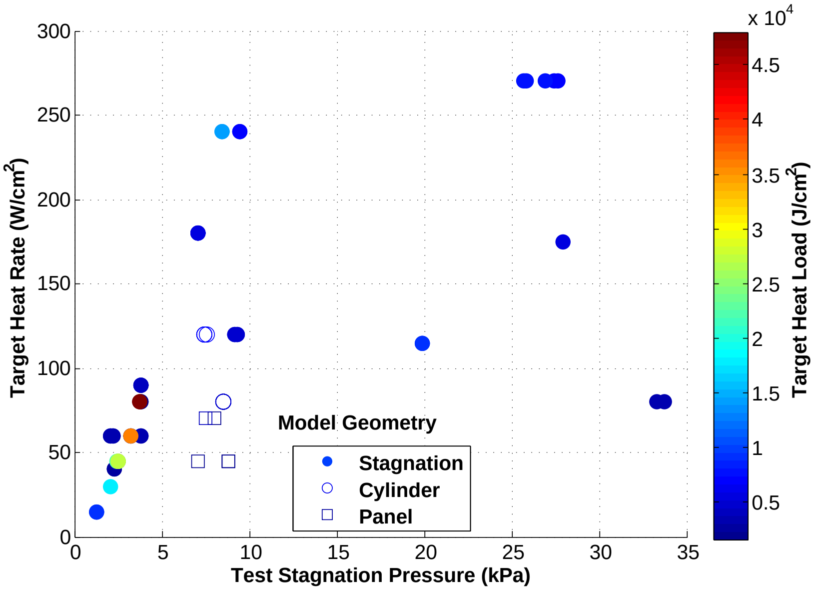

Figure 3.1: Scope of MEDLI test campaign illustrating model geometries, target cold-wall heat flux, target heat load, and stagnation pressure

remainder of this chapter describes the methods used to analyze the PICA experimental thermal response compared with simulated response using this database.

3.3 Analysis method and statistics

Mahzari et al. [37] used MEDLI flight data to compare material response predictions from NASA's MR code FIAT [17] with entry data. They applied the temperatures of the near-surface thermocouples as boundary conditions to FIAT. This technique, called the "TC driver" method, solves the in-depth heat conduction equations using near-surface thermocouple measurements to anchor the solution. Using this type of modeling, only the internal heat conduction problem and pyrolysis problem are considered, which minimizes many of the uncertainties introduced by the boundary layer assumptions [43, 44], as well as the arc jet operating conditions (for instance, enthalpy) [45–47]. The method does not incorporate surface heat flux, radiation, recession, or the myriad of other phenomena which would need to be considered to apply an aero-heating boundary condition. The simplification provides the advantage of decoupling the material response from uncertainties in surface conditions and surface model assumptions [10, 36]. Direct comparisons can then be made with other thermocouple measurements taken deeper within the TPS test article. The work presented here uses the TC driver method to compare FIAT predictions with the compiled MEDLI arc jet test data.

A total of six temperature profile comparisons can be made for every MISP, each containing four thermocouples. The top TC, called the "driving" TC, is used as a boundary condition and the comparisons can be made with all lower TCs, called "reference" TCs. For example, when the top "driving" TC (TC1) is used, the predicted thermal response can be compared using TC2, TC3, and TC4. Next, TC2 can be used as the temperature boundary condition, and comparisons made using TC3 and TC4, and likewise for TC3 boundary condition. For example, Figure 3.2 shows Test 302 performed in the Aerodynamic Heating Facility (AHF) with all of the possible TC driver configurations.

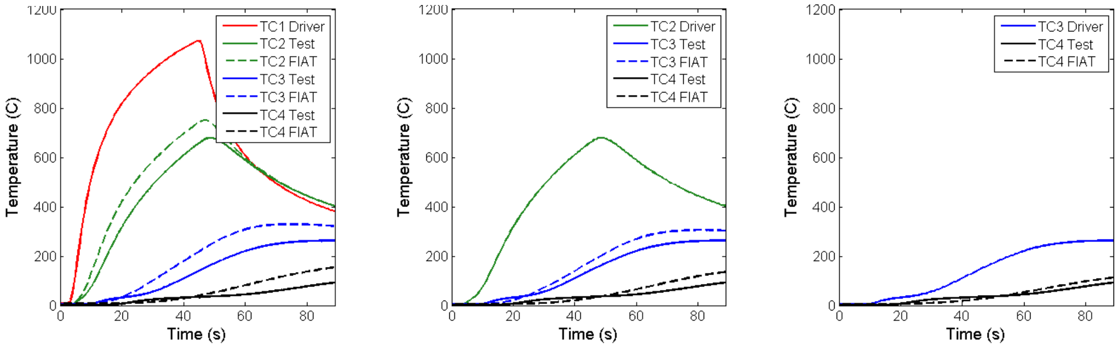

(a) TC1 driving, results compared to TC2, TC3 and TC4

(b) TC2 driving, results compared to TC3 and TC4

(c) TC3 driving, results compared to TC4

Figure 3.2: FIAT predictions with measured data for MISP stagnation model in Aerodynamic Heating Facility test series 302 for 40s flow exposure

The analysis of the experimental MISP data was performed using the 1D material response code FIAT version 3.0 [17, 48] with the material database for PICA (in-air) version 3.3. The FIAT material response model requires pressure and temperature inputs to calculate the appropriate thermal properties such as thermal conductivity and heat capacity. This pressure is assumed to be uniform through the depth of the material and in time. For each test, pressure port data obtained during each calorimeter run was referenced from the database. The full “material stack-up” behind the TPS material is recorded along with test start time and end time in the database (Table 3.1).

Because 65 MISPs were analyzed using this methodology, quantitative measurements are proposed in order to reduce and summarize the extensive results. This allows for a statistical approach to be applied rather than simply inspecting temperature profiles visually, like those seen in Figure 3.2. Equations 3.1 to 3.4 define the parameters used to compare the experimental and modeled results while Figure 3.3 gives a visual representation of each metric.

$$\text{Peak Error} = \max(T_F) - \max{}_i(T_M). \tag{3.1}$$

$$\text{Peak Percentage Error} = \frac{\max(T_F) - \max_i(T_{i,M})}{\max(T_M) + 273.15} \tag{3.2}$$

$$\text{Max Difference} = \max|T_F - T_M| \tag{3.3}$$

$$\text{Deviation} = \sqrt{\frac{\sum_i (T_F - T_M)^2}{N}} \tag{3.4}$$

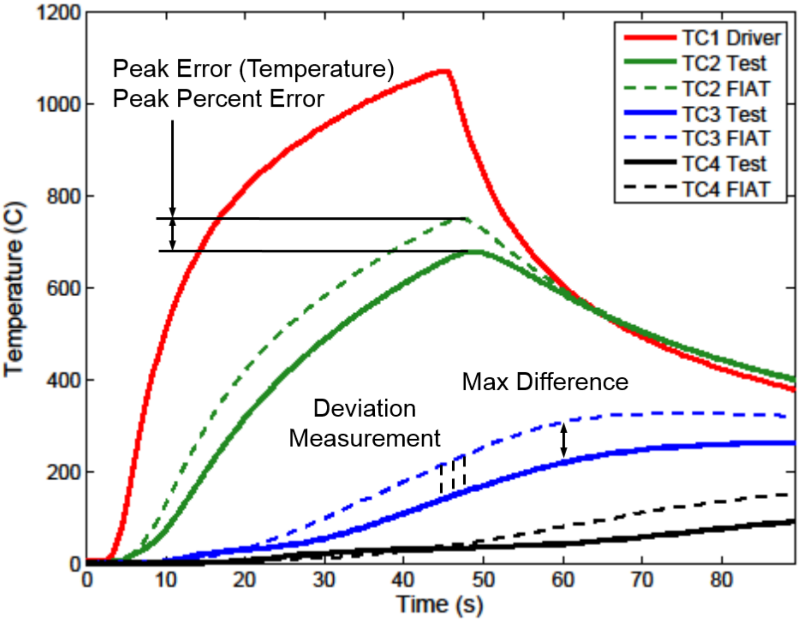

Figure 3.3: MEDLI arc jet series AHF Test 302 Run 005 showing parameters used for FIAT TC1 driver simulation and comparison for standard MISP plug

In these equations: i is the sample index, N is the number of samples through the test duration, and T_F and T_M are the temperature output from FIAT and the measured temperature respectively for each time i. These parameters were chosen to reflect the significance of maximum temperature, an important design criterion, as well as a temporally integrated difference (called *Deviation*). For some of the parameters, using different sampling frequencies from one test to another is a concern. Since the different arc jet facilities and test plans called for different sampling frequencies, measurements must be interpolated to the same time discretization to accurately calculate parameters such as the *Maximum Difference* and *Deviation*.

3.4 Results and discussion

The metrics described in Section 3.3 were calculated for 65 MISPs used in the arc jet ground test facilities. Since each MISP has six possible "driving" to "reference" combinations, a large sample size allows for comparing many combinations of the conditions described in Table 3.1. The results for each TC driving combination are shown as an individual histogram, each of which shows the distance between the "driving" and "reference" thermocouple as well as the mean and standard deviation of the distribution of the calculated parameter.

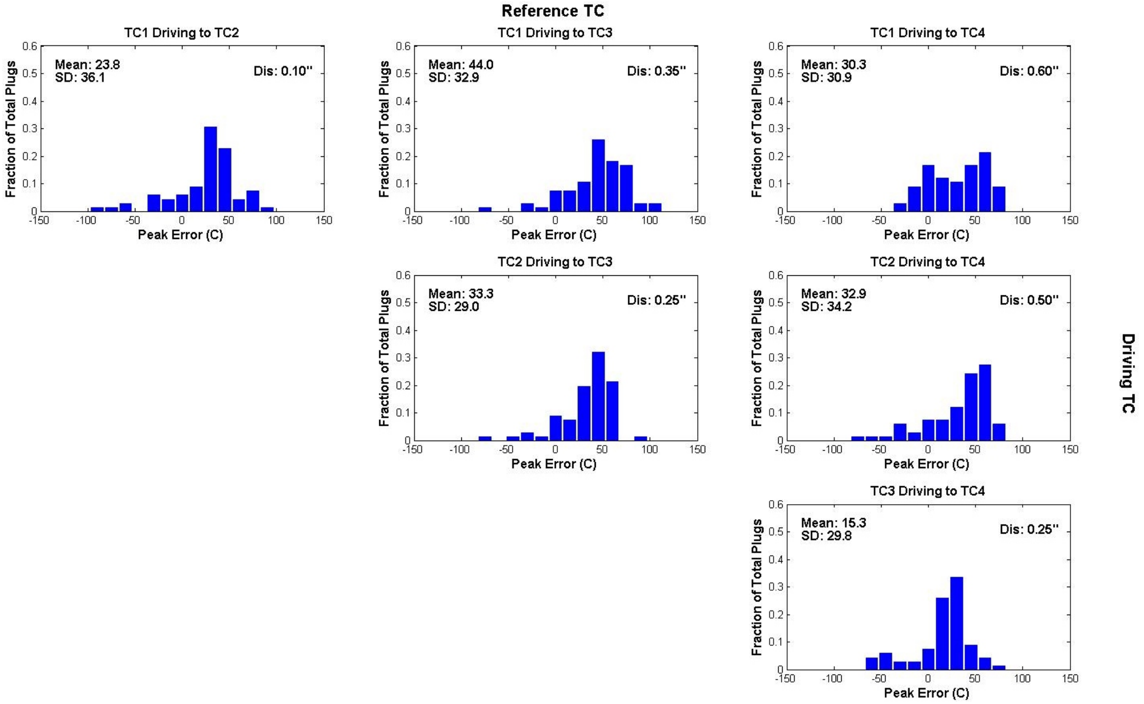

Figure 3.4: Histograms of Peak Temperature Error (Eq. 3.1) from measured temperature separated by location of driving and reference thermocouple for 65 MEDLI PICA plugs

From Figure 3.5, it was found that distance between the "driving" thermocouple and "reference" thermocouple is very significant to the material response modeling.

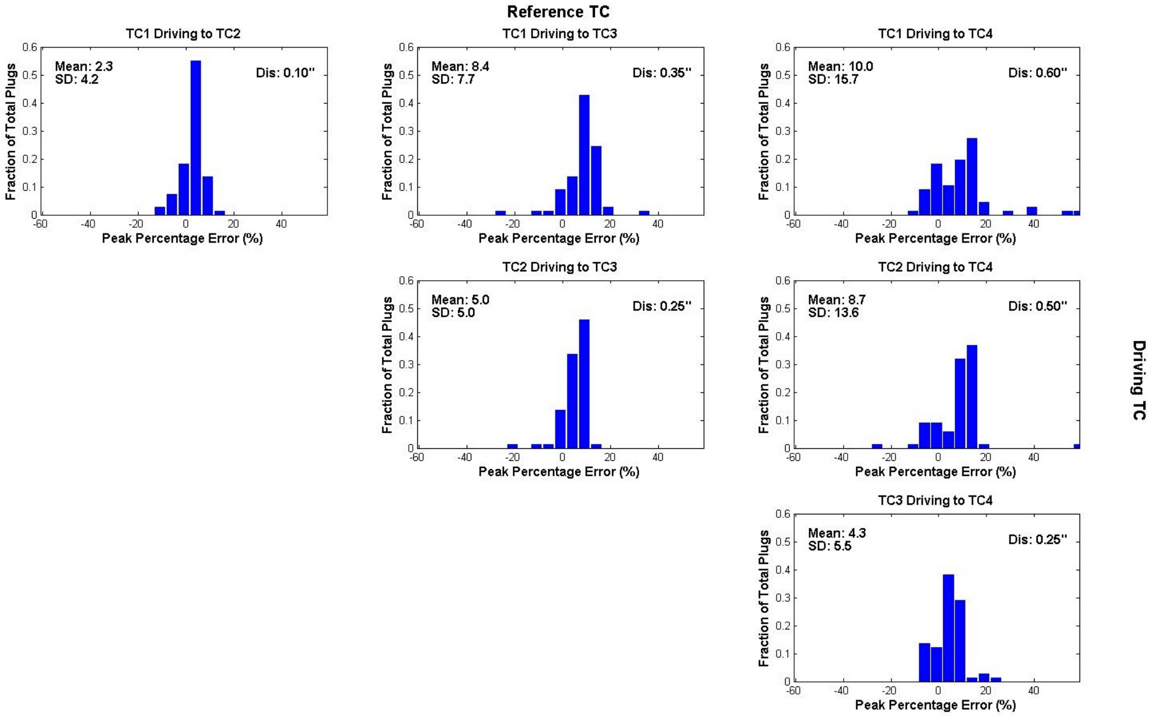

Figure 3.5: Histograms of Peak Temperature Error (Eq. 3.2) as percent error from measured temperature separated by location of driving and reference thermocouple for 65 MEDLI PICA plugs

Specifically, as this distance increases, the peak temperature error increases significantly. From the smallest driving distance to the largest, both the mean and standard deviation increase by around a factor of four. This means that the accuracy of the material response conduction model for PICA is highly correlated with the thickness of the TPS models, or more specifically, the thickness in which the conduction is taking place when comparing TC data. These results are clearly seen in the *Deviation* measurement (Figure 3.7), which captures the temperature differences over the integrated test duration. It is also expected that deeper thermocouples have greater dependence on the test model geometry. That is, 2D conduction effects will affect deeper thermocouples more [9, 13, 49].

From Figs. 3.4 to 3.7, various additional observations can be made. For instance, the TC1 driving to TC2 histogram shows the accuracy of the char properties since the peak temperatures for TC1 and TC2 typically occur above pyrolysis tempera-

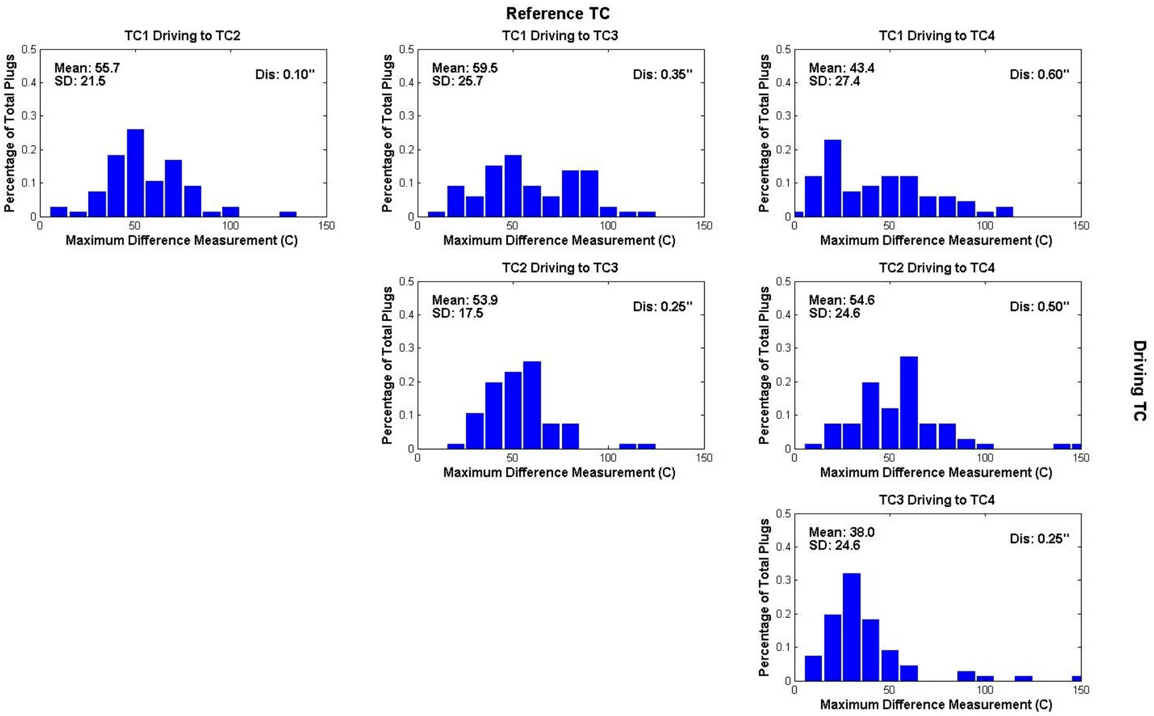

Figure 3.6: Histograms of Maximum Difference (Eq. 3.3) from simulated to measured temperature separated by location of driving and reference thermocouple for 65 MEDLI PICA plugs

tures. Similarly, the TC3 driving to TC4 histogram shows the accuracy of the virgin model since the peak temperatures for TC3 and TC4 typically occur below pyrolysis temperatures. As seen in Figure 3.7, the FIAT predictions within this region provide the lowest deviations where fewer physical high-temperature phenomena are taking place or are being modeled. The TC1 driving to TC4 incorporates the char, pyrolysis, and virgin properties across a greater distance, and larger deviations measurement are observed.

3.5 Limitations, bias, and remarks

The described method of data analysis comprises various limitations and assumptions. Many parameters vary across the test series, such as the severity of the test conditions or change in model geometry. For example, in Figure 3.8, differences seen from installation method were compared using the *Peak Percentage Error*. Al-

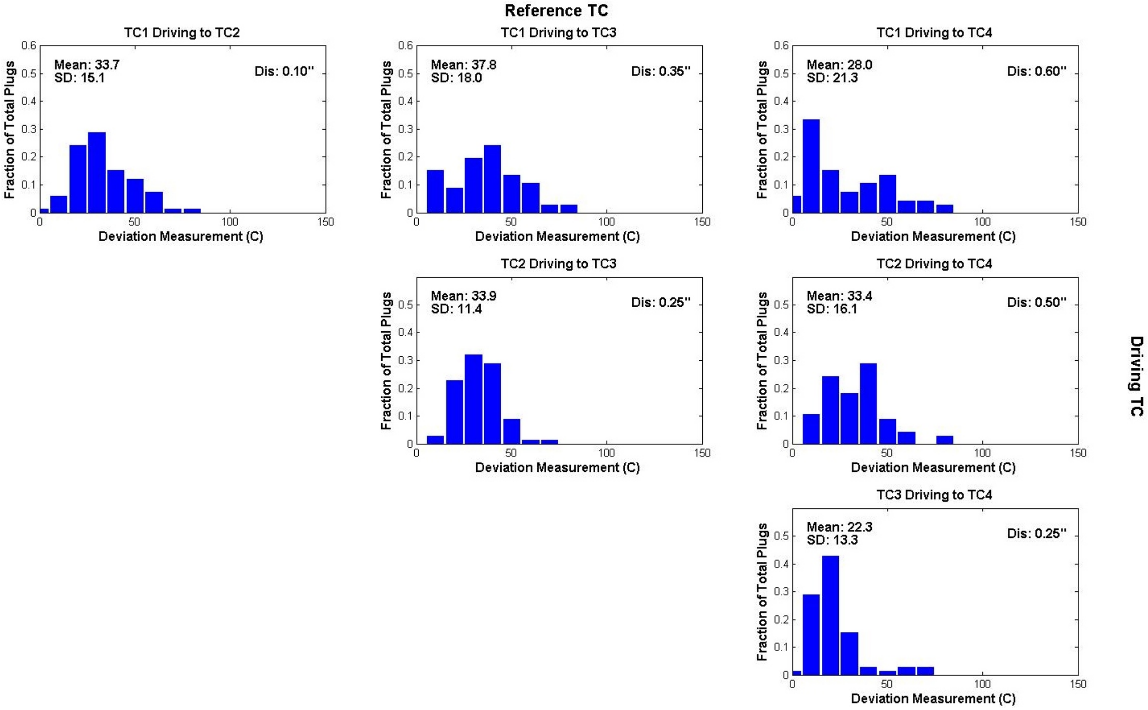

Figure 3.7: Histograms of Deviation (Eq. 3.4) from measured temperature separated by location of driving and reference thermocouple for 65 MEDLI PICA plugs

though more outliers are present in the RTV bonded plug sample, it appears that the installation method does not affect the accuracy of the material response model. The outliers could be a result of the fact that more RTV bonded plugs were tested in the initial qualification test series which typically involved more severe test conditions than later series.

Another example is the diameter of the test articles, which affect the amount of sidewall heating seen by internal thermocouples. The heat conducted between two thermocouples could therefore be misrepresented when using a 1D material response approach [9, 13, 49]. Other uncertainties are present as well, one of which being the PICA material properties. From the information in the database, nearly all of the MISPs were manufactured using the same PICA billet, and it is known that material properties differ not only from one billet to another but also within a billet. The material properties used in this work are representative of the average PICA properties [29, 50]. Moreover, since the material surrounding the MISPs came from different

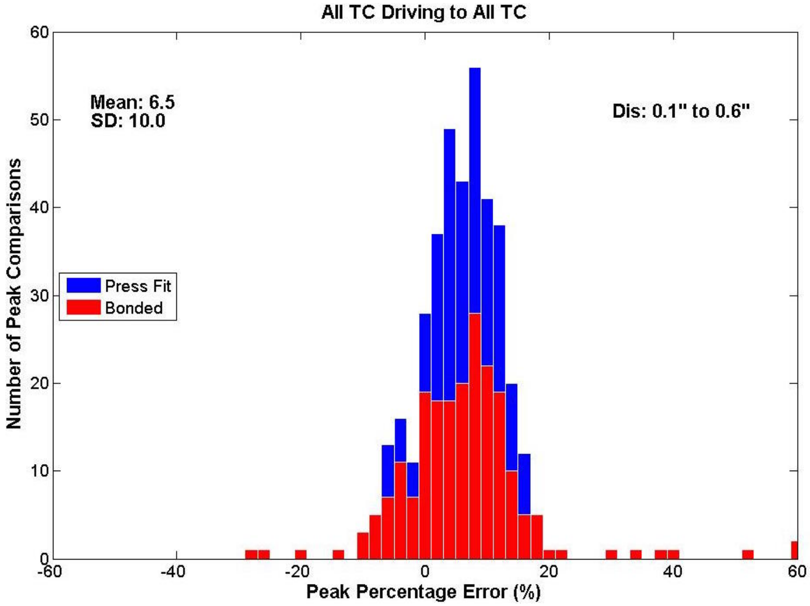

Figure 3.8: Stacked histogram of Peak Temperature Error as percent error (Eq. 3.2) from measured temperature for 65 MEDLI PICA plugs of different installation methods with all TC driving combinations

billets, discrepancies could be caused by this difference. As a result, comparing across multiple billets is beneficial on a macro scale, and caution should be used with regard to billet variability while comparing individual tests.

Many tests were exposed to extreme heating conditions for long periods of time. As a result, the ablation front moved past the near-surface thermocouples which exposed them to temperatures well above $1250\,°C$, outside the calibration range of type-K thermocouples. These temperatures can even be reached far before the ablation front reaches the TC. When this occurs, the thermocouple data becomes extremely erratic and inutile. Therefore, only test data beneath $1250\,°C$ were modeled using the TC driver approach. This naturally creates a bias in many of the calculations obtained. For instance, the peak error percentage from Eq. 3.2 uses the maximum temperature during the test, but when the TC exceeds $1250\,°C$, the simulation is stopped, and the error is calculated at that point. From the trends observed in the prediction and experimental temperature profiles, it appears that this bias has little effect on the difference in the two maximum temperatures even though the metric is captured below the true maximum temperature obtained. For thermocouples where $1250\,^{\circ}C$ is not reached, a time window that is three times longer than the model exposure time is used. As a result, the deviation parameter has a bias introduced by the cool-down time. Another source of error in the deviation parameter is the influence of possible inaccuracies during the beginning of the FIAT simulation which would negatively affect temperature predictions later in time. For all of these reasons, conclusions should be based on multiple parameters as a conglomerate rather than individually. Despite these biases, much agreement shown in terms of test-to-test consistency as demonstrated by Figure 3.8 being symmetric, unimodal, and bell-shaped.

In more than 90% of the tests models, evidence of the low-temperature "hump" phenomenon was observed in the temperature histories. The "hump" is a change in concavity in the temperature profile and can be seen in Figs. 3.2 and 3.3. The material response tools used in this study do not incorporate this behavior, and therefore, large errors between the measured and simulated temperatures are seen in this regime. This phenomenon was also not predicted with the flight data using the same TC driving technique [37]. Using the MEDLI arc jet database, further analysis of the "hump" phenomenon has been performed. The analysis, as well as a preliminary model, is presented in Chapter 4 [38].

Future studies like these can provide additional insights by using alternative comparison techniques and models than those described in this work. For example, using models that capture surface recession or 3D heating effects to make comparisons with the assembled database would be of particular interest.

The MEDLI arc jet database provides a resource of large sample size to analyze and compare experimental results and material response models. With this information and resulting analysis, future instrumentation projects similar to MEDLI will require less testing.

The work presented shows quantitative and extensive measurements regarding the relationship between current model prediction capabilities and measured test results for PICA samples. An example of such analysis is the estimations for the error seen in maximum temperature and the total error for different regions of the TPS. The results indicate that current prediction capabilities using a one-dimensional material response model tend to overpredict the experimental maximum temperatures by an average of 6.5%. Moreover, as TPS thickness increases, modeling temperatures at the "bondline" from surface or near-surface conditions become less accurate.

The large-scale direct comparison of model simulations with ground test data are useful to TPS engineers; in particular, variation and predictability in temperature performance of ablators can be used to make informed decisions around uncertainties and design margins. For these reasons, the MEDLI arc jet database provides an important resource for both instrument designers and ablation modelers.

Chapter 4 Effects of Water Presence on Low-Temperature Phenomenon in Porous TPS Materials

4.1 Overview and hypothesis

A low-temperature phenomenon was consistently observed through thermocouple measurements deep within the TPS material during the MEDLI flight and arc jet testing. Figure 2.3 shows the measured MSL flight temperature response along with the predicted temperature profiles at the thermocouple depths. It can be seen that the estimated heating environment and the material response model shows significant differences with the flight data, namely an unexpected change in concavity occurred in deeper thermocouple responses, called the “hump.” The modeled results do not predict any change in concavity in this low-temperature regime. It is proposed that the observed “hump” is a result of the heat of vaporization during the endothermic phase transition of the water within the TPS material. This hypothesis is supported by the known absorption of water by PICA and other carbon-phenolic porous materials from the atmosphere prior to testing or flight [30].

In the proceeding sections of this chapter, the effects of a liquid-to-vapor water phase transition within the TPS material are explored and supporting evidence is presented. Because water phase transition is believed to be the major contributor to this phenomenon, other possible effects of water presence are temporarily neglected in order to simplify the model. Some of these potential factors may include changes in heat capacity, thermal conductivity, and gas phase equilibrium. The low-temperature “hump” phenomenon seen in multiple carbon phenolic ablators is recreated within a material response code by implementing a water phase transition model. The work compiled here illustrates supporting evidence to the hypothesis that water is causing the irregularity seen for in-depth temperature profiles.

4.2 Experimental cases and supporting evidence

MEDLI arc jet testing

Mahzari et al. [37] discussed the unexpected temperature "hump" in the lower thermocouple temperature profiles of the MSL flight data, and noted how it was observed in all of the MISP locations, but did not postulate a possible explanation. Seen in Figure 2.4, the "hump" is not accurately predicted using the thermocouple driver approach, and therefore, comparisons to measured thermocouple data in this temperature regime show substantial deviations in temperature. Current material response models fail to predict the temperature profile concavity change using the TC driver method, meaning errors exist within the conduction modeling techniques. The work of Mahzari et al. provides a strong impetus for solving the "hump" problem, implying that the use of in-depth thermocouple data is limited for other applications until this phenomenon is correctly modeled.

During the development of the MEDLI suite, extensive arc jet testing was performed at NASA Ames Research Center on PICA test articles with the embedded thermocouples units. These tests were collected in a database in which material response predictions could be compared [39]. In these tests, the "hump" phenomenon within the material was consistently observed by the deepest thermocouples (the ones further from the surface), clearly identified in over 90% of the 65 test articles, and very similar to that found in the MSL flight data [38]. An analytical method using a thermocouple boundary approach to estimate material properties similar to that conducted by Mahzari et al. [37] was implemented and ignored the "hump" effect when determining material properties, as there was no available explanation for the behavior at the time [37]. The phenomenon occurred around 310 K, which is in the same temperature regime seen during Mars entry. One such example can be seen in Figure 4.1 of a test completed in the Interaction Heating Facility which shows typical "hump" behavior and the thermocouple boundary approach with FIAT. Note that the "hump" response is rarely observed in near-surface thermocouples, but this likely due to the high-temperature gradients in the near-surface region, which could obscure or conceal an evanescent "hump" due to the higher heat fluxes in that region and potentially unsteady heating conditions seen early in typical test windows.

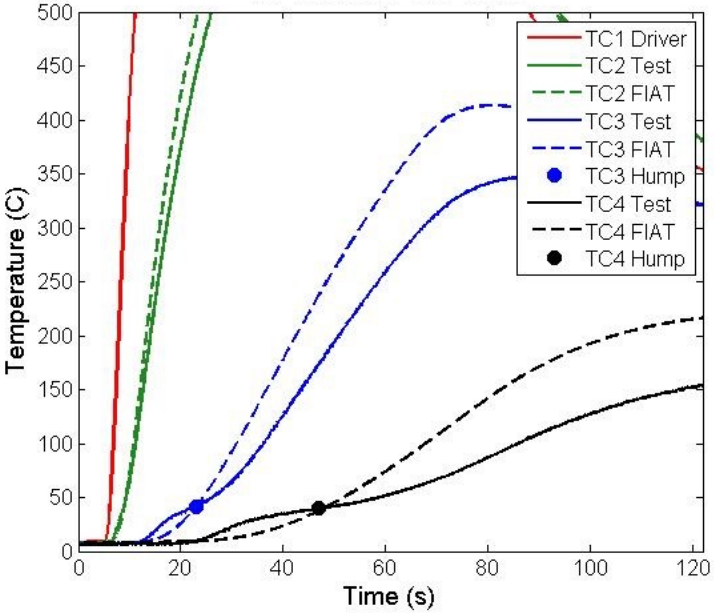

Figure 4.1: MEDLI arc jet series IHF Test 253 Run 008 showing low-temperature hump with FIAT TC1 driver simulation for standard MISP plug

The "hump" temperatures, when defined as a local minimum in the temperature gradient, observed during the MEDLI test series, correlate well with the known saturation curve of water when plotted against the test article stagnation pressure as seen in Figure 4.2.

During a particular arc jet ground test series in NASA Ames Research Center's Aerodynamic Heating Facility (AHF), thermocouples recorded the "hump" occurring

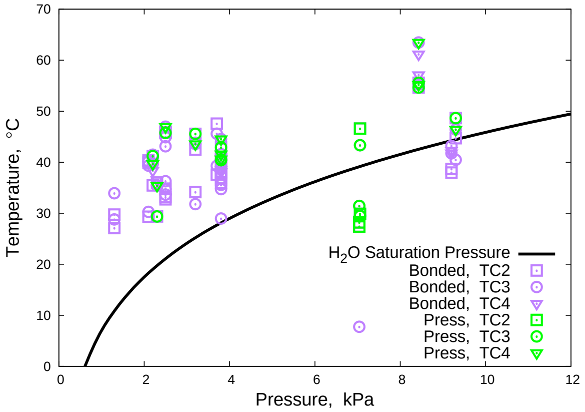

Figure 4.2: "Hump" temperatures for MEDLI arc jet testing in comparison to saturation curve of water

at different temperatures. During these tests, the MISPs were installed using two different methods: half of them involved RTV, a vulcanized silicone sealant, around the thermocouples (bonded), and the other half without any sealant (press-fit). Three pairs of each article type were tested at the same arc jet conditions. All of the RTV bonded models experience higher "hump" temperatures than their non-bonded model pairs as seen in Figure 4.3. It is noted that the initial temperatures of the plugs are offset due to ambient heating in the test chamber; that is, the bonded models were inserted into the flow after the press-fit models, and their temperatures increased during the interim. The initial temperature difference is not believed to cause a change in the "hump" temperature because other MEDLI testing with liquid nitrogen-soaked models did not show significant effects on the phenomenon's characteristics.

Under the assumption that the RTV sealant limits transverse gas flow through the porous carbon phenolic and thus increases the local pressure around the thermocouples, this test case supports the proposed hypothesis. Because water phase transition is highly dependent on pressure, any water within an RTV bonded plug would evaporate at a higher temperature as observed. An example of transverse gas flow in an Iso-Q geometry TPS model is shown in Figure 4.4.

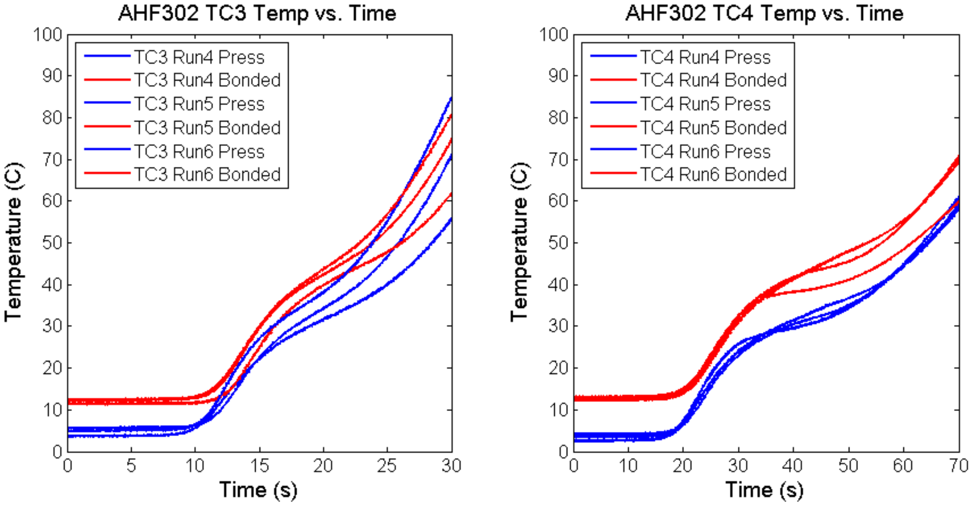

Figure 4.3: AHF 302 low thermocouple response with press-fit and RTV sealed plugs

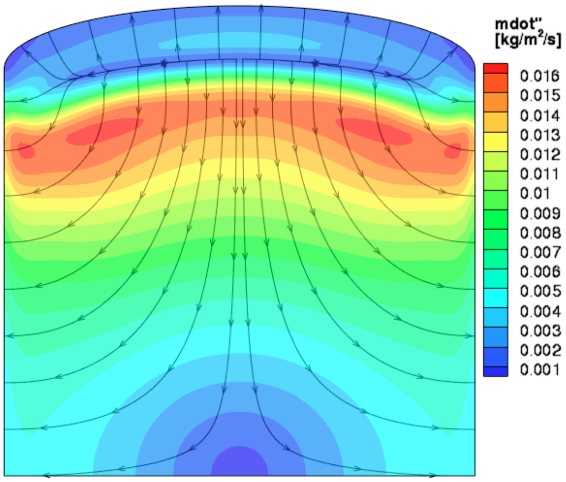

Figure 4.4: Sample Iso-Q heating case with transverse mass flow from Kentucky Aerodynamic and Thermal-response System (KATS). Image from Ref. [7].

Additional arc jet ground test cases

Kobayashi et al. [8] shows test results for low-density ablators that are heated in arc jet wind tunnels with nitrogen and air test gases. Various measurements are taken on the test sample including material density, surface temperatures, and most importantly, in-depth temperatures. The arc jet testing was carried out in two wind tunnels in Japan at the Institute of Aerospace Technology of Japan Aerospace Exploitation Agency and at Japan Ultra-high Temperature Materials Research Center [8].

The test article used is a carbon phenolic ablator which is fabricated by impregnating a resin into a carbon fiber felt and has a virgin density between 0.23g/cm^3 and 0.27g/cm^3. This material is in the same family of material as the PICA used for the MEDLI suite discussed previously. A fraction of the models were instrumented with type K thermocouples at locations 10, 15, and 30 mm downstream from the surface, while other models have thermocouples mounted at 5, 10, and 15 mm from the surface. Kobayashi et al. [8] explains a progressive machining technique that is used post-test on the models in order to obtain a density profile and presents the raw density values. Also, comparisons of the effective heat of ablation is made between that of PICA and the low-density ablator used in this test.

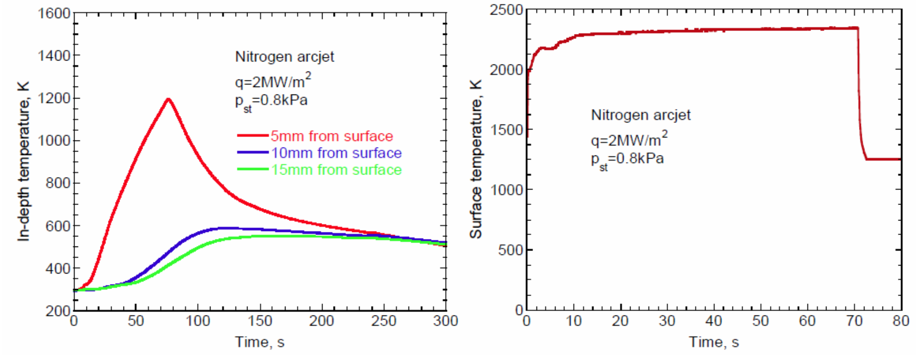

Figure 4.5: Test results from nitrogen arc jet testing. Image from Ref. [8].

From the work presented, the results from the in-depth thermocouples are of particular interest. Figure 4.5 shows the temperature profiles with respect to time for the arc jet test in Nitrogen. Although the low-temperature "hump" phenomena is not discussed in this presented work, it is clearly seen in the results presented at the same temperature regime as observed in other test and flight cases as a change in concavity of the temperature profile. The "hump" can even be seen briefly in the thermocouple closest to the surface, which is not the case in the MISP test plugs. The shape and contour of the "hump" appears very similar to previously discussed and presented cases. The temperature results essentially level out during the test. It should be noted that the upper TC "hump" could be caused by unsteady heating conditions, but the flow conditions are in steady state when the lower TCs "hump" transitions. The "hump" is also clearly seen in other tested models by Kobayashi et al. [8] in Figure 4.6 and 4.7 which are tested at significantly different heating rates.

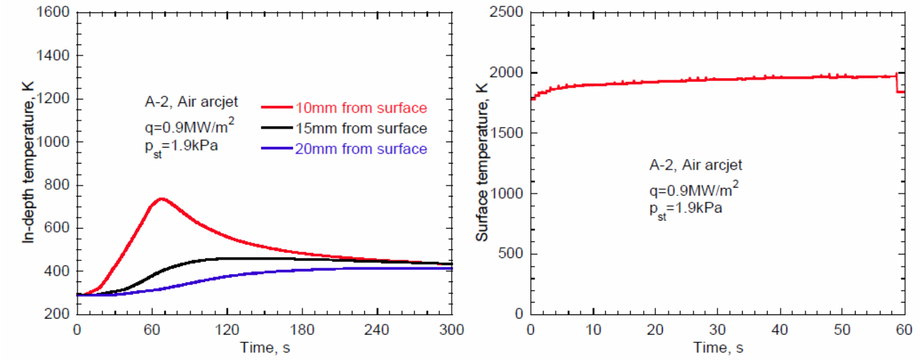

Figure 4.6: Test results from air arc jet testing with low heat flux. Image from Ref. [8].

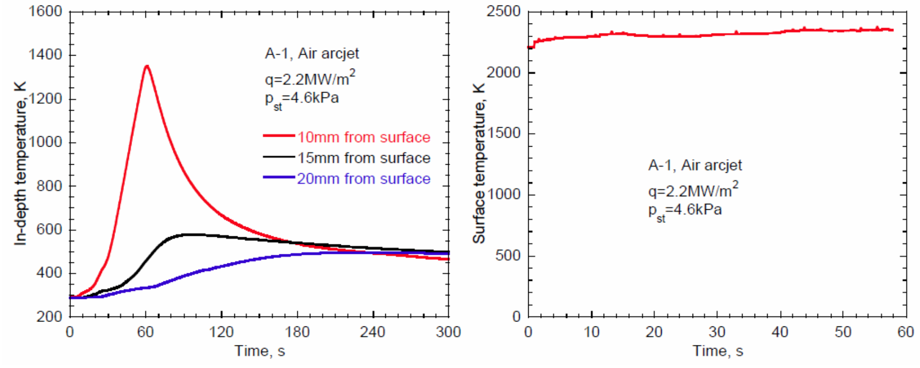

Figure 4.7: Test results from air arc jet testing with high heat flux. Image from Ref. [8].

The presented test case is further evidence that the "hump" is likely caused by a universal phenomenon, because the material used is different than the PICA cases discussed earlier. One possible such phenomenon is carbon-phenolic's known tendency to absorb water from the atmosphere at room temperature. It should be noted that the there is no discussion on pre-test practices, and it is unknown if efforts were made to hold the test article at low pressures before the duration of the test. This could minimize the chances of liquid water being present in the material when the test begins, but even if this is the case, or some other measure is taken which contradicts the theory that water is cause the temperature "hump," it is still very significant that the phenomenon is occurring with separate TPS materials in various arc jet facilities around the world. With this evidence, the possibility that the "hump" is caused by an instrumentation anomaly associated with NASA's facility of the MISP manufacturing process is dismissed.

The phenomenon is also seen using other TPS materials such as AVCOAT. Both the Orion EFT-1 flight and arc jet thermocouple data in AVCOAT ablator showed a similar low-temperature response [30, 32] and a carbon-phenolic material used by Kobayashi et al. [8] during experimental arc jet ground tests. The effect is also apparent in deeper thermocouple data for Mars Pathfinder [34] which used SLA-561V, a silicone- and cork-based ablator in a phenolic honeycomb matrix. This suggests that the phenomenon is not a result of instrumentation error or testing anomaly since it is seen consistently in various flight and test conditions.

4.3 Modeling

The finite-volume code used in this work is called Kentucky Aerodynamic and Thermal-response Solver (KATS) [49], and the material used is Theoretical Ablative Composite for Open Testing (TACOT) [51]. TACOT is used instead of PICA because it has similar properties and is an open-source material while the distribution of PICA material properties remains limited [29]. Because TACOT properties are not exactly the same as those of PICA, MEDLI data is not expected to be matched exactly, but the changes of in-depth temperature trends from the water vaporization model are intended to sufficiently replicate the "hump" nevertheless.

As a first step, liquid water phase transition is implemented by adding a set of additional mass conservation equations in the material response. The purpose of the model is not to capture the myriad of complicated physics involved with multi-phase porous media flow, but to look specifically at the phase change influence on the energy equation, and its effects on material temperature. However, since many of the test initial conditions begin in the liquid domain, a solid water species is not considered here. The model is easily extendable to the solid water case with an additional mass conservation equation of similar form to that of liquid water.

The general conservation form of equations can be written as:

$$\frac{\partial \mathbf{Q}}{\partial t} + \nabla \cdot (\boldsymbol{\mathcal{F}} - \boldsymbol{\mathcal{F}}_d) = \mathbf{S} \tag{4.1}$$

Using backward Euler method and spatial integration, the following linear system is thus solved for each control volume, at each time step:

$$\left[\frac{V}{\Delta t} \frac{\partial \mathbf{Q}}{\partial \mathbf{P}} - \frac{\partial \mathbf{R}HS}{\partial \mathbf{P}} \right] \Delta \mathbf{P} = -\sum_{\text{faces}} (\boldsymbol{\mathcal{F}} - \boldsymbol{\mathcal{F}}_d) \cdot \mathbf{n} A + \mathbf{S} V \tag{4.2}$$

The right hand side of Eq. (4.2) is designated as **RHS**, such that,

$$\mathbf{RHS} \equiv -\sum_{\text{faces}} (\boldsymbol{\mathcal{F}} - \boldsymbol{\mathcal{F}}_{\mathbf{d}}) \cdot \mathbf{n} A + \mathbf{S} V \tag{4.3}$$

and $\mathbf{P}$, $\mathbf{Q}$, and $\mathbf{S}$ are vectors of primitive variables, conservative variables, and source terms, respectively. $\boldsymbol{\mathcal{F}}$ and $\boldsymbol{\mathcal{F}}_d$ are the matrices of convective and diffusive flux, respectively.

The governing equations are represented by the following vectors and matrices including the additional water conservation equations [49]:

$$\mathbf{Q} = \begin{pmatrix} \phi\rho_g \\ \rho_{s_1} \\ \rho_{s_2} \\ \rho_{s_3} \\ \xi_{w_l} \\ \xi_{w_v} \\ \phi\rho_g u \\ \phi\rho_g v \\ \phi\rho_g w \\ \phi E_g + E_s + E_w \end{pmatrix}, \qquad \mathbf{P} = \begin{pmatrix} \phi\rho_g \\ \rho_{s_1} \\ \rho_{s_2} \\ \rho_{s_3} \\ \xi_{w_l} \\ \xi_{w_v} \\ u \\ v \\ w \\ T \end{pmatrix}, \qquad \mathbf{S} = \begin{pmatrix} \omega_g \\ \omega_{s_1} \\ \omega_{s_2} \\ \omega_{s_3} \\ \omega_{w_l} \\ \omega_{w_v} \\ D_x \\ D_y \\ D_z \\ S_D \end{pmatrix}, \tag{4.4}$$

$$\boldsymbol{\mathcal{F}} = \begin{pmatrix} \phi\rho_g u & \phi\rho_g v & \phi\rho_g w \\ & & \\ & \mathbf{0} & \\ & & \\ \phi\rho_g u^2 + p & \phi\rho_g vu & \phi\rho_g wu \\ \phi\rho_g uv & \phi\rho_g v^2 + p & \phi\rho_g wv \\ \phi\rho_g uw & \phi\rho_g vw & \phi\rho_g w^2 + p \\ \phi\rho_g uH & \phi\rho_g vH & \phi\rho_g wH \end{pmatrix}, \qquad \boldsymbol{\mathcal{F}}_d = \begin{pmatrix} \\ \mathbf{0} \\ \\ \mathbf{F}_{cond} \end{pmatrix}. \tag{4.5}$$

where ξ_{w_l} and ξ_{w_v} are the mass of liquid water and water vapor divided by the cell volume. The relationship can be expressed by

$$\xi_{w_l} = \rho_{w_l}\frac{V_w}{V}, \qquad \xi_{w_v} = \rho_{w_v}\frac{V_w}{V} \tag{4.6}$$

where ρ_{w_l} and ρ_{w_v} are the densities of liquid water and water vapor respectively, V_w is the volume occupied by the water mass, and V is the total sample volume.

Solid Decomposition Model

For solid species, a phenomenological three-components model is used [52] with the addition of a water species. The addition of a water species is a successive step in the modeling approach. The total solid density is computed independently from the water presence and is computed by

$$\rho_s = \sum_{i=1}^{3} \Gamma_i \rho_{s_i} \tag{4.7}$$

where Γ_i is the volume fraction of species i in the virgin composite. As with standard TACOT material modeling, the intermediate properties are interpolated from the virgin and char states. The decomposition rate of each original solid component is given by:

$$\omega_{s_i} = \frac{\partial \rho_{s_i}}{\partial t} = -A_i \rho_{v i} \left(\frac{\rho_{s i} - \rho_{c_i}}{\rho_{v_i}} \right)^{\psi_i} \exp\left(-\frac{E_i}{RT} \right), \qquad T > T_{react_i}, \tag{4.8}$$

where subscript v and c are respectively for virgin and char state of the solid material.

Water Phase Change Model

The heat of vaporization for water is captured by the conservative energy term E_w, which is formalized in manner described in Eq. (4.9).

$$E_w = \sum_{i=1}^{2} \xi_{w_i} h_{w_i} = \xi_{w_l} h_{w_l} + \xi_{w_v} h_{w_v} \tag{4.9}$$

Using this technique, as the modeled water changes phase from liquid to gas, the total increase in internal energy is captured from the difference in liquid and vapor enthalpy [53]. In the implemented model, liquid water is assumed to be present within the TPS, and liquid density throughout the entire grid is specified as an initial condition. Next, mass balance equations for water density are proposed in order to enforce the phase change from liquid to vapor. The physics behind liquid vaporization may involve, and is not limited to, boiling phenomenon, convection of inner gas flow, and shapes of initial water droplet presence. However, these effects are difficult to model, and a simplified reaction equation is proposed, as shown in Eq. (4.10). This simplified approach is not necessarily physical, but for the scope of this work, it serves as an effective way to model the phase-change process. That is, as the material exceeds the saturation temperature of water, rapid phase change is enforced based on both the remaining water density and the current cell temperature.

$$\omega_{w_l} = \frac{\partial \xi_{w_l}}{\partial t} = -A_w \xi_{w_l} \left(\frac{T - T_{sat}}{T_{sat}} \right), \qquad T > T_{sat}\left(p\right) \tag{4.10}$$

The pressure dependence of the saturation temperature is the most critical aspect of the reaction rate equation, and its dependence is well known [53]. Eq. (4.11) is constructed under the conservation of mass assumption for all water species.

$$\omega_{w_v} = \frac{\partial \xi_{w_v}}{\partial t} = -\frac{\partial \xi_{w_l}}{\partial t} = -\omega_{w_l} \tag{4.11}$$

Eqs. (4.9) to (4.11) fully define the water model added to the original material response model as seen in Eq. (4.5). Results are calculated for various mass fractions of water and boundary conditions similar to that found in ground arc jet cases [39]. This is the only way in which the modeled water interacted with the phenolic structure and porous media flow, through energy conservation, and thus the temperature influence. The remaining system is left unaltered by the water presence in the material, and future work is intended to further define this coupling by modeling any complex interactions between the water, phenolic, and gas species.

Gas and Mixture Energy Model

In this model, the pyrolysis gases are treated as a single gas species under an equilibrium assumption with properties obtained via equilibrium calculations. In KATS, the gas transport is solved in a distinct momentum equation, which is a time-dependent version of Darcy's law, [49] while the mixture energy equation assumes the gas, solid, and water are in thermal equilibrium. The solid decomposition and pyrolysis gas generation ensure total mass conservation. For simplicity, within the implemented model, the produced water vapor is not transported within the porous material with the other gases. Further implementation will support the water vapor transport and, under certain conditions, re-condensation to the liquid or solid state deeper within material.

Boundary Conditions

Simulations begin by using one-dimensional analysis. Then, in order to replicate the arc jet ground tests, a cylindrical geometry is used with both the heat flux boundary conditions and fixed temperature boundary conditions. Using a 3D geometry allows for simulation of the press-fit and bonded plugs by controlling the sidewall characteristics and assuming that press-fit plugs have permeable sides and that bonded plugs are impermeable. These boundary conditions are shown in Figure 4.8 for a cylindrical geometry.

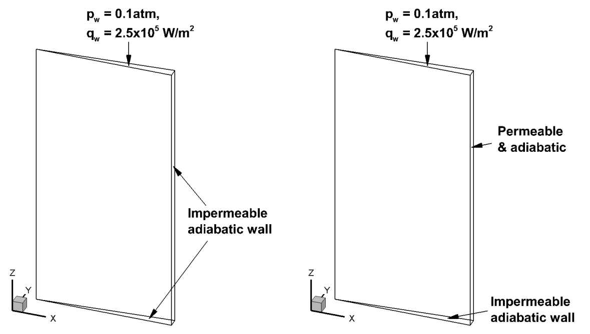

(a) Impermeable sidewall case

(b) Permeable sidewall case

Figure 4.8: Computational geometry and boundary conditions for the cylinder case

In this analysis, a wedge-shaped grid uses axisymmetric conditions along $x = 0$ m to simulate a cylinder. Figures 4.9 and 4.10 show that the internal pressure is significantly correlated with sidewall permeability [9]. The lower pressures in Figure 4.10 compared to those in 4.9 (b) are a result of gas flow through the permeable wall at

$x = 0.05$ m. For the impermeable case, the pressure is significantly higher because the gas products have a more constricted path.

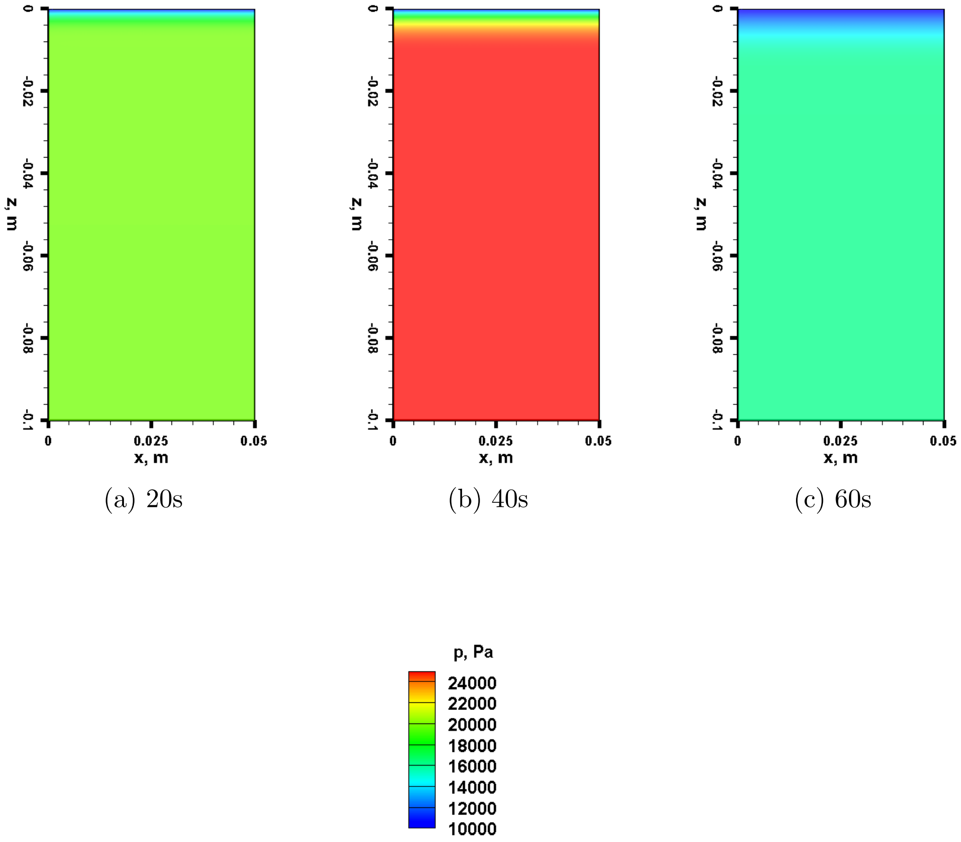

(a) 20s (b) 40s (c) 60s

Figure 4.9: Pressure contours of impermeable sidewall cylinder for 40s exposure to 25 W/cm^2 heat flux at 0.1 atm with the radial coordinate x [9].

4.4 Results

Temperature profiles are calculated as a function of time at specific depths within the modeled 1D geometry. The present initial effort is intended to recreate the general shape of the temperature profile with little focus on exact curve traces to match the

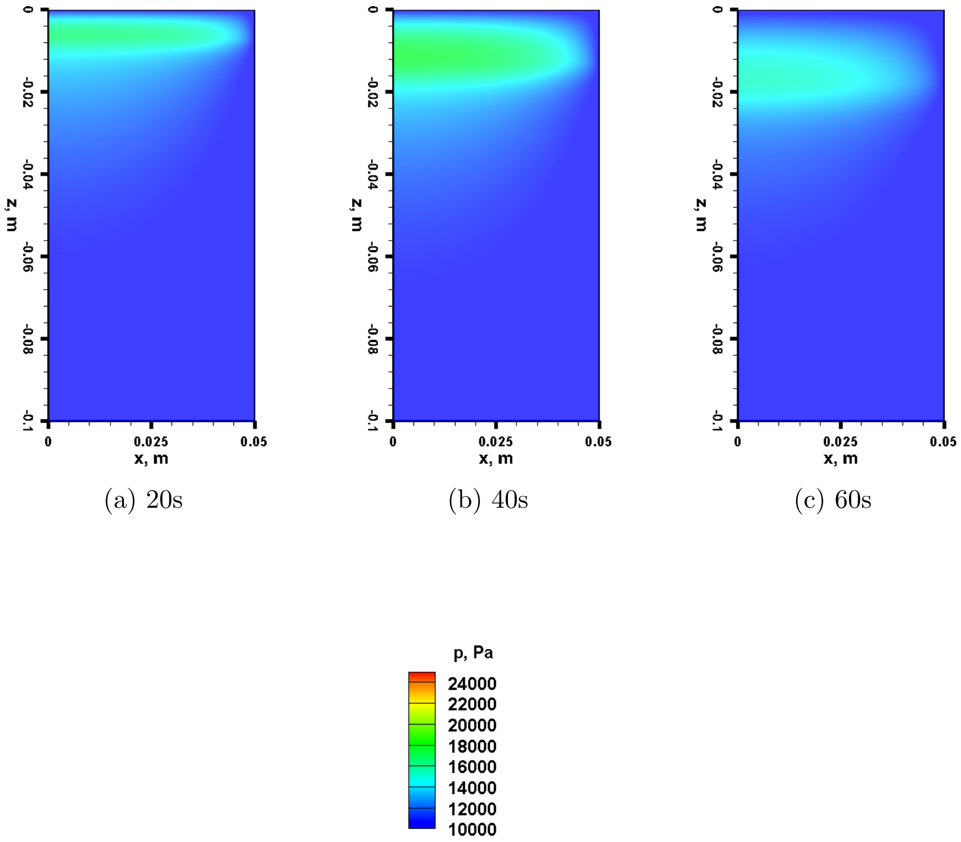

(a) 20s (b) 40s (c) 60s

Figure 4.10: Pressure contours of permeable sidewall cylinder for 40s exposure to 25 W/cm^2 heat flux at 0.1 atm with the radial coordinate x [9].

experimental data. Because of the differences between TACOT and PICA, an exact match is not expected. The cases presented have water in an initial liquid phase and are compared to the cases with identical heating conditions and thermocouple locations with zero water presence.

Effects of Internal Water Densities

From Figure 4.11, it is clearly seen that the temperature trend is influenced by the initial water presence. These results are to be expected from the addition of the

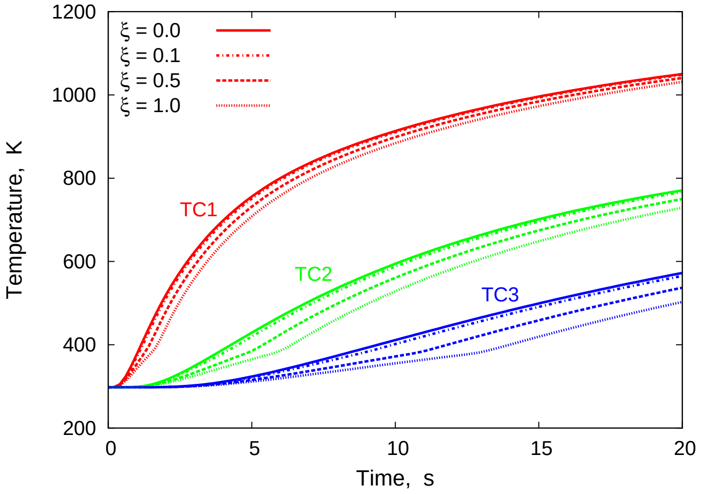

Figure 4.11: 1D water model with surface temperature boundary condition of 1500K at 1 atm with variable water densities. ξ is the liquid water mass per unit volume in kg/m^3.

water thermal mass and the energy change introduced to the system. Various mass fractions of water are evaluated in Figure 4.11, which indicates as the amount of water is increased, internal temperature rise is impeded. By implementing the initial condition of $\xi_{w_l} = 1$ throughout the material, the total virgin mass of TACOT is increased about 0.4%. This is well within the mass increase of 1-2% observed for PICA samples from ordinary atmospheric exposure [30].

Reaction Rate Coefficient Effects

As the only control parameter in the current water vaporization model proposed in Eq. (4.10), the reaction rate coefficient A_w controls the vaporization speed from liquid to gas phase. The higher A_w value is, the shorter time it takes for water to vaporize and the smoother the temperature change is near the saturation temperature, as shown in Figure 4.12. Also, below the saturation temperature, less heat is transferred into the material. Because the temperature profile is sensitive to this parameter, future work will involve choosing the correct value for A_w, or changing the reaction rate method all together.

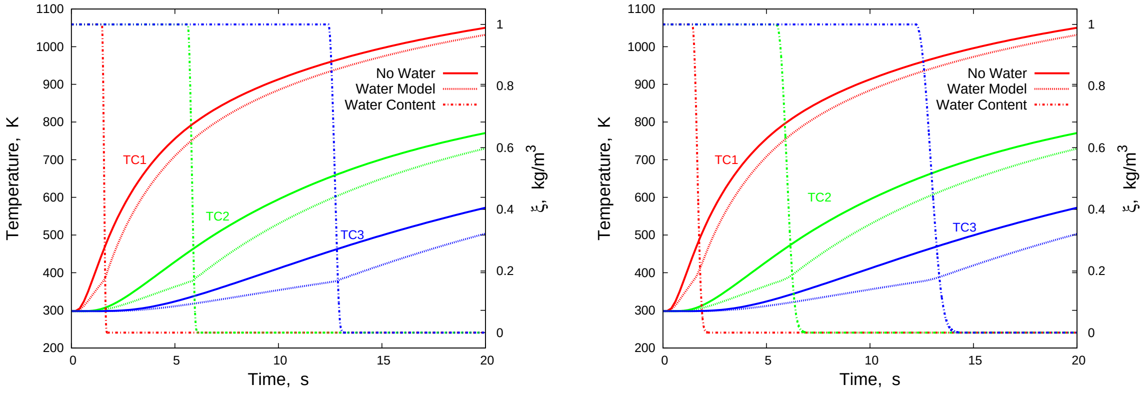

(a) $A_w = 1000\ s^{-1}$ (b) $A_w = 100\ s^{-1}$

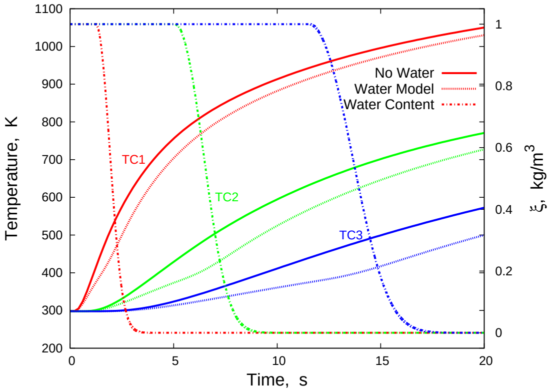

(c) $A_w = 10\ s^{-1}$

Figure 4.12: 1D water model with surface temperature boundary condition of 1500K at 1 atm using variable ration rate coefficients

Pressure Dependence

From Figure 4.3, the “hump” temperature is expected to be influenced by the plug installation method: press-fit or bonded. Under the assumption that the RTV surrounding the bonded plugs is impermeable, the presented hypothesis is further supported by Figs. 4.9 and 4.10, which show how the internal pressure is significantly correlated with sidewall permeability. Because vaporization temperature is a strictly increasing function of pressure (Figure 4.2), plugs with impermeable RTV bonding experience higher “hump” temperatures, which are in agreement with the experimental data. Figure 4.13 shows how the present model is effected by different pressures. The boundary condition of $P = 0.1$ atm is of the order of the measured surface pressures from the AHF 302 test series [39]. The results show how the effects of phase transition are shifted to lower temperatures comparable to those of the observed, experimental "hump".

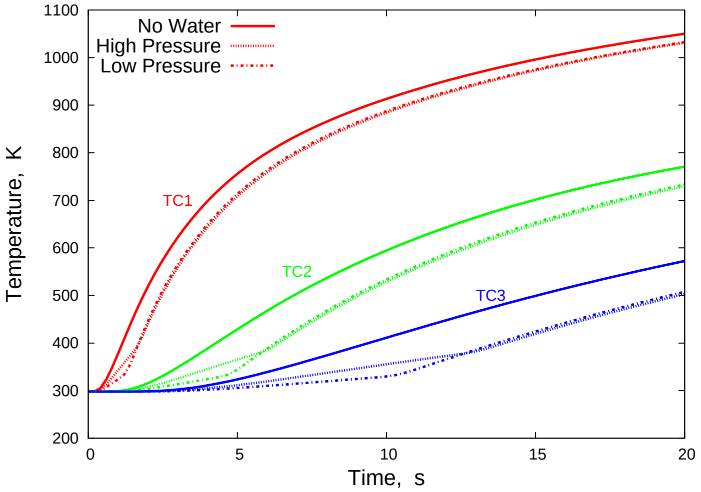

Figure 4.13: 1D water model with surface temperature boundary condition of 1500K at 1 atm and 0.1 atm

3D Model with Boundary Condition Modification

Considering the experimental results shown in Figure 4.3 and the 3D boundary condition study shown in Figs. 4.9 and 4.10, the water phase transition model was implemented with a 3D geometry in order to replicate the effects of a permeable-wall press-fit plug and an impermeable-wall RTV bonded plug. These plotted temperature profiles are for thermocouple locations along the centerline of the material.

For Figure 4.15, it is evident that the impermeable sidewall conditions lead to higher internal temperatures than that of the permeable case, which is consistent with Ref. 13. However, these effects appear to be minimal in the low-temperature region where the "hump" occurs. For this case, the "hump" temperature is not significantly altered by the wall boundary conditions because local pressure is not effected as it is in Figure 4.13. The pressure effects do not occur in this model until higher temperatures are reached.

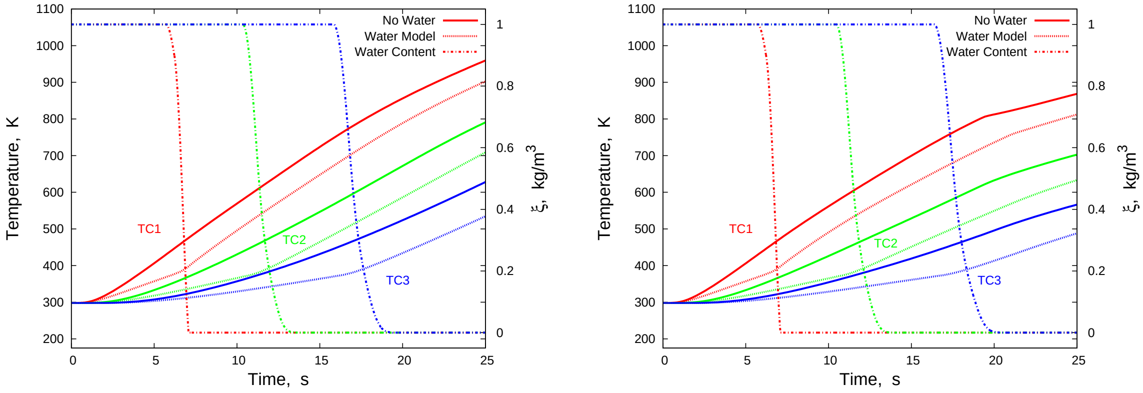

(a) Permeable sidewall (b) Impermeable sidewall

Figure 4.14: Temperature profiles for 3D water model with surface heat flux boundary condition of 10 W/cm^2 at 1 atm for centerline TC locations

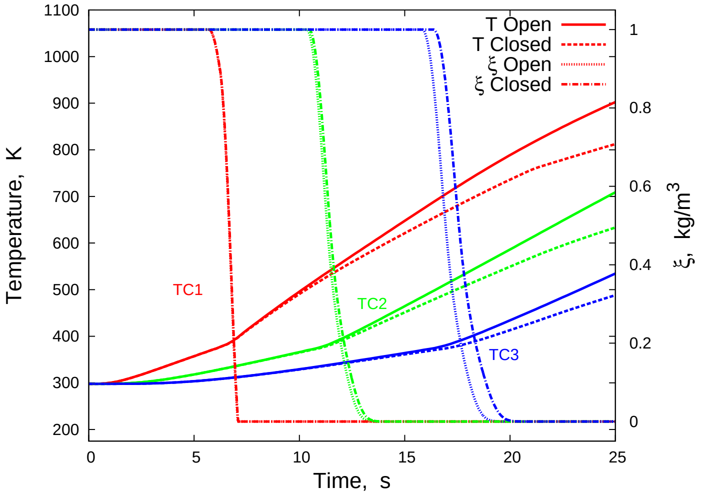

Figure 4.15: Temperature profile comparisons for 3D water model with surface heat flux boundary condition of 10 W/cm^2 at 1 atm for centerline TC locations showing both permeable and impermeable sidewall

Although the 3D case results do not correlate with the AHF 302 experiment as well as expected, the presented hypothesis is still plausible and probable. This is mainly justified by the known water absorption and presence in PICA and other ablative materials in which the "hump" is observed [8, 32]. In addition, the change of the thermal conductivity due to the water presence is also believed to contribute towards the "hump" profile. In particular, an increase in thermal conductivity from the liquid water could facilitate additional heat transfer and cause the temperature to rise before phase change, potentially more accurately matching the experimental "hump" profile. The temperature profiles in the "hump" region are most likely also effected by the thermal conductivity of the water.

Thermal Conductivity Modification

As previously discussed, another likely significant influence on the "hump" production is the increase in thermal conductivity of the TPS in regions with a liquid water presence. A preliminary model explores these effects using the following modification to the conductivity results.

$$\lambda = \lambda_s + \psi\lambda_{w_l}, \qquad \psi = \frac{\xi_{w_l}}{2\xi_w} \tag{4.12}$$

Where λ_s is the solid carbon phenolic thermal conductivity and λ_{w_l} is the thermal conductivity of liquid water at the local temperature. The thermal conductivity is only modified for the liquid regime because pure liquid water has a thermal conductivity an order of magnitude larger than that of water vapor. Using this model, a recognizable "hump" is seen in the precise temperature region of experimental results. It should be noted that the thermocouple locations were specified further from the grid surface for this case in order to observe meaningful differences from those of previous results.

Fig 4.16 more closely replicates the experimental measurements of the "hump" phenomenon by increasing the temperature prior to phase transition while the temperature gradient tends to decrease in this region as well. Fig 4.16 indicates how the two different aspects of the model influence results in the "hump" temperature region. Without the conductivity modification, the profile is shifted and the change in temperature gradient is observed. In contrast, as the conductivity modification is implemented, additional heat transfer is facilitated during liquid phase. Although these results begin to show expected results from water implementation, additional

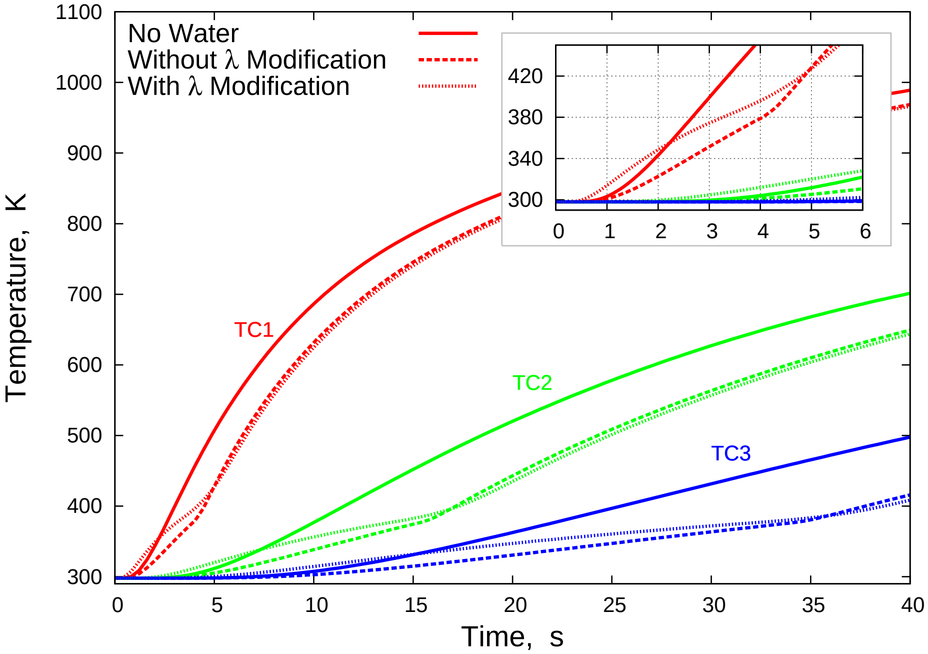

Figure 4.16: 1D water model with surface heat flux boundary condition of 50 W/cm^2 at 1 atm using ration rate coefficient A=100

physics needs to be implemented in order to properly model the presence of water in ablative TPS.

Chapter 5 Conclusion

The Mars Science Laboratory Entry Descent and Landing Instrumentation project performed extensive arc jet tests for development, qualification, and calibration of instrumented heat shield plugs. These plugs each contained several thermocouples for measuring near-surface and in-depth temperature response of the phenolic impregnated carbon ablator. The arc jet test results have been compiled into a comprehensive database so that broad trends across the test series can be compared and analyzed over a variety of test conditions. Furthermore, the MEDLI arc jet database acts as a resource of large sample size to analyze and compare experimental results and material response models. With the information compiled into the database and resulting quantitative analysis, future instrumentation projects similar to MEDLI will require less testing. The large-scale direct comparison of model simulations with ground test data are useful to TPS community; in particular, variation and predictability in temperature performance of ablators can be used to inform uncertainties and design margins. For these reasons, the MEDLI arc jet database provides an important resource for both instrument designers and ablation modelers.

One of the analysis methods studied is the comparison of ablator material response calculations that solve the in-depth heat conduction equations. Using the near-surface thermocouple measurements as a boundary condition in numerical simulations, comparisons are made with other thermocouple measurements taken deeper within the TPS test article. This technique is used to compare test results with model simulations using several quantitative metrics, such as such as peak-temperature difference, maximum difference in temperature, and a total integrated temperature deviation. The work presented shows these quantitative and extensive measurements regarding the relationship between current model prediction capabilities and measured test results for PICA samples. A significant difference in prediction behavior with respect to the location of source thermocouple is shown based on these comparisons.

The temperature prediction accuracy is quantified for the tested material and material response code and is found to be highly dependent on the distance between the boundary condition thermocouple and the deeper reference thermocouple. Overall, the one-dimensional material response model tends to overpredict the experimental maximum temperatures by an average of 6.5%. Moreover, as TPS thickness increases, modeling temperatures at the "bondline" from surface or near-surface conditions become less accurate. Based on this test analysis, it is shown that numerical models can predict in-depth temperature measurements equally well for sensor plugs installed in the arc jet test model with or without a silicone adhesive. It is found that predicted temperatures are consistently greater than measured values indicating the PICA material model is generally conservative for in-depth temperature predictions.

In addition, a low-temperature phenomenon was consistently observed through thermocouple measurements deep within the material during the MEDLI arc jet testing. This anomaly, referred to here as the "hump", consists of a change in concavity of the temperature profile well below the maximum temperature and is seen in various TPS materials and atmospheric conditions, and typically occurs around 40 °C. The "hump" temperatures in the MEDLI test series correlate well with the known saturation curve of water when plotted against the stagnation pressure. It is proposed that the observed "hump" is a result of the heat of vaporization during the endothermic phase transition of water within the TPS material. This is supported by the known absorption of water by PICA from the atmosphere prior to testing or flight. The presented material response model captures energy effects of phase transition from a pre-existing water presence. This work shows that water presence currently appears to be the most probable cause for the phenomenon, which is observed in multiple different porous TPS materials. Additional modifications can further be made to the ablation model which account for the other implications of water presence, such as changes in thermal conductivity, diffusivity, porosity, and gas phase equilibrium.

The effects of water presence on temperature trends in porous TPS materials are explored thoughout this work. Because a temperature concavity change has been consistently observed among multiple TPS materials within a predictable range, it is believed that the cause of the phenomenon is not system specific. The concavity change occurs near the phase transition temperature of water. Since porous ablator materials, such as PICA, are known to absorb water from the atmosphere, has been theorized that the low-temperature "hump" in the thermocouple data is a result of water phase transition. Because the "hump" has not been previously modeled in any existing material response codes, a novel model to account for the effects of the water presence was proposed. Using a surrogate ablator material, TACOT, a series of numerical studies were performed to study the effects of the proposed model, using the material response module of KATS solver. The results of the studies captured the change of temperature profiles due to the presence of water, since water vaporization absorbs heat. In addition, the change in temperature gradient with respect to time is reproduced near saturation temperature, as was seen in the experimental thermocouple data. Several important sensitivities were noted, namely the rate at which liquid water turns to water vapor.

Possible areas of improvement in the modeling include thermal conductivity effects, solid phase change for frozen water in flight, thermal capacitance, and water vapor transport within the material. Additionally, ground test experiments with measured water content of various concentrations could greatly contribute to the understanding of these effects. Despite the fact that the current model does not fully reproduce the "hump" phenomena, the results show a promising direction in the water effect modeling.

This work has shown that including water phase transition in the energy balance can alter in-depth material temperatures. Because heat shield design involves sizing the ablator so that in-depth bondline temperatures stay below a design limit, it is therefore important to further investigate the effects of water and phase transition on ablator performance. Further improvements in TPS modeling, including water phase transition and increased confidence levels in modeling capabilities, may support reductions in the TPS mass of future entry vehicles.

Bibliography

[1] Amar, A. J., Blackwell, B. F., and Kuznetsov, A. V., *Modeling of One-Dimensional Ablation with Porous Flow Using Finite Control Volume Procedure*, Master's thesis, North Carolina State University, May 2006.

[2] "MSL Entry Rendering," `https://www.nasa.gov/centers/ames/images/content/671686main_msl_reenty_full.jpg`, Accessed: 2016.

[3] Bose, D., Olson, M., Laub, B., White, T., Feldman, J., Santos, J., Mahzari, M., MacLean, M., Dufrene, A., and Holden, M., "Initial Assessment of Mars Science Laboratory Heatshield Instrumentation and Flight Data," *51st AIAA Aerospace Sciences Meeting*, AIAA Paper 2013-908, Grapevine, TX, January 7-10 2013.

[4] White, T., Mahzari, M., Bose, D., and Santos, J. A., "Post-flight Analysis of the Mars Science Laboratory Entry Aerothermal Environment and Thermal Protection System Response," *AIAA*, January 2013.

[5] Lachaud, J. and Mansour, N. N., "Porous-material Analysis Toolbox based on OpenFOAM-extend and Applications," *AIAA 2013-2767*, June 2013.

[6] Mahzari, M., Braun, R. D., White, T., and Bose, D., "Inverse Estimation of the Mars Science Laboratory Entry Aerothermal Environment and Thermal Protection System Response," *44th AIAA Thermophysics Conference*, AIAA Paper 2013-908, June 2013.

[7] Weng, H. and Martin, A., "Numerical Investigation of Pyrolysis Gas Blowing Pattern and Thermal Response using Orthotropic Charring Ablative Material," *AIAA 2014-2121*, 2013.

[8] Kobayashi, Y., Sakai, T., Suzuki, T., Fujita, K., Okuyama, K., Kato, S., and Kitagawa, K., "An Experimental Study on Thermal Response of Low Density Carbon-Phenolic Ablators," *Journal of Spacecraft and Rockets*, Januaryr 2009.

[9] Weng, H., Bailey, S. C. C., and Martin, A., "Numerical study of iso-Q sample geometric effects on charring ablative materials," *International Journal of Heat and Mass Transfer*, Vol. 80, January 2015, pp. 570–596.

[10] Martin, A. and Boyd, I. D., "Modeling of heat transfer attenuation by ablative gases during the Stardust re-entry," *Journal of Thermophysics and Heat Transfer*, Vol. 29, No. 3, July 2015.

[11] Amar, A. J., Blackwell, B. F., and Edwards, J. R., "One-Dimensional Ablation Using a Full Newton's Method and Finite Control Volume Procedure," *Journal of Thermophysics and Heat Transfer*, Vol. 22, No. 1, January 2008, pp. 72–82.

[12] Amar, A. J., Blackwell, B. F., and Edwards, J. R., "Development and Verification of a One-Dimensional Ablation Code Including Pyrolysis Gas Flow," *Journal of Thermophysics and Heat Transfer*, Vol. 23, No. 1, January–March 2009, pp. 59–71.

[13] Weng, H. and Martin, A., "Multidimensional modeling of pyrolysis gas transport inside charring ablative materials," *Journal of Thermophysics and Heat Transfer*, Vol. 28, No. 4, October–December 2014, pp. 583–597.

[14] Lachaud, J. and Mansour, N. N., "Porous-Material Analysis Toolbox Based on OpenFOAM and Applications," *Journal of Thermophysics and Heat Transfer*, Vol. 28, No. 2, April 2014, pp. 191–202.

[15] Amar, A. J., Calvert, N. D., and Kirk, B. S., "Development and Verification of the Charring Ablating Thermal Protection Implicit System Solver," *49th AIAA Aerospace Sciences Meeting*, AIAA Paper 2011-144, Orlando, FL, Jan. 4-7 2011.

[16] van Eekelen, T., Bouilly, J.-M., Hudrisier, S., Dupillier, J.-M., and Aspa, Y., "Design and numerical modelling of charring material ablators for re-entry applications," *Proceedings of the Sixth European Workshop on Thermal Protection Systems and Hot Structures*, European Space Agency - WPP-319, University Stuttgart, Germany, 21-25 November 2009.

[17] Chen, Y.-K. and Milos, F. S., "Ablation and Thermal Response Program for Spacecraft Heatshield Analysis," *Journal of Spacecraft and Rockets*, Vol. 36, No. 3, May-June 1999, pp. 475–483.

[18] Nompelis, I., Drayna, T. W., and Candler, G. V., "A Parallel Unstructured Implicit Solver for Hypersonic Reacting Flow Simulation," *17th AIAA Computational Fluid Dynamics Conference*, AIAA Paper 2005-4867, Toronto, ON, 2005.

[19] Martin, A., Scalabrin, L. C., and Boyd, I. D., "High performance modeling of an atmospheric re-entry vehicles," *Journal of Physics: Conference Series*, Vol. 341, No. 1, February 2012, Article 012002.

[20] Wright, M. J., Candler, G. V., and Bose, D., "Data-Parallel Line Relaxation method for the Navier-Stokes equations," *AIAA Journal*, Vol. 36, No. 9, September 1998, pp. 1603–1609.

[21] Zhang, H., *Coupling of high temperature gas and porous media flow*, Ph.d. thesis, University of Kentucky, Lexington, KY, August 2015 (Expected).

[22] "Seeing red," *Nature*, Vol. 479, No. 7374, November 2011, pp. 446–446.

[23] Tran, H. K., Johnson, C. E., Rasky, D. J., Hui, F. C. L., Hsu, M.-T., and Chen, Y. K., "Phenolic Impregnated Carbon Ablators (PICA) for Discovery class missions," *31st AIAA Thermophysics Conference*, AIAA Paper 1996-1911, New Orleans, LA, June 17-20 1996, pp. 1–14.

[24] Santos, J. A., Oishi, T., and Martinez, E. R., "Isotherm Sensor Calibration Program for Mars Science Laboratory Heat Shield Flight Data Analysis," *42nd AIAA Thermophysics Conference*, AIAA Paper 2011-3955, Honolulu, HI, 27 - 30 June 2011, pp. 1–10.

[25] Gazaric, M., Wright, M., Little, A., Cheatwood, F. M., Herath, J., Munk, M., Novak, F., and Martinez, E., "Overview of the MEDLI Project," *Aerospace Conference, 2008 IEEE*, No. IEEE Paper 2008-1510, Big Sky, MT, 3-10 March 2008, pp. 1–12.

[26] Driver, D. M., Carballo, J. E., Beck, R., Prabhu, D., Santos, J. A., Cassell, A., Skokova, K., Tang, C., and Hwang, H. H., "Arc Jet Testing in a Shear Environment for Mars Science Laboratory Thermal Protection System," *41st AIAA Thermophysics Conference*, AIAA Paper 2009-4230, San Antonio, TX, 22 - 25 June 2009, pp. 1–18.

[27] Bose, D., Santos, J. A., Rodriguez, E., White, T. R., and Mahzari, M., "Mars Science Laboratory Heat Shield Instrumentation and Arc Jet Characterization," *44th AIAA Thermophysics Conference*, AIAA Paper 2013-2778, June 24-27 2013, pp. 1–18.

[28] Lachaud, J., Magin, T. E., Cozmuta, I., and Mansour, N. N., "A short review of ablative-material response models and simulation tools," *7th European Symposium on Aerothermodynamics*, Brugge, Belgium, 2011.

[29] Milos, F. and Chen, Y.-K., "Ablation and Thermal Property Model for Phenolic Impregnated Carbon Ablator (PICA)," Technical Memorandum 2009-215377, NASA Ames Research Center, Moffett Field, CA, March 2009.

[30] White, T., personal communication, May 2015.

[31] Curry, D. M. and Stephens, E. W., "Apollo Ablator Thermal Performance at Superorbital Entry Velocities," Tech. Rep. NASA TN D-5969, Manned Spacecraft Center, Houston, Texas, September 1970.

[32] Bose, D. and Mahzari, M., personal communication, Feb. 2015.

[33] Spencer, D. A., Blanchard, R. C., Braun, R. D., Kallemeyn, P. H., and Thurman, S. W.

[34] Milos, F. S., Chen, Y.-K., Congdon, W. M., and Thornton, J. M., "Mars Pathfinder Entry Temperature Data, Aerothermal Heating, and Heatshield Material Response," *Journal of Spacecraft and Rockets*, Vol. 36, No. 3, 1999, pp. 380–391.

[35] Trumble, K. A., Cozmuta, I., Sepka, S., Jenniskens, P., and Winter, M., "Post-flight Aerothermal Analysis of Stardust Sample Return Capsule," *AIAA 2009-1587*, September-October 2010.

[36] White, T. R., Mahzari, M., Bose, D., and Santos, J. A., "Post-flight Analysis of the Mars Science Laboratory Entry Aerothermal Environment and Thermal Protection System Response," *44th AIAA Thermophysics Conference*, AIAA Paper 2013-2779, San Diego, CA, June 24-27 2013, pp. 1–19.

[37] Mahzari, M., Braun, R. D., White, T. R., and Bose, D., "Inverse Estimation of the Mars Science Laboratory Entry Aeroheating and Heatshield Response," *Journal of Spacecraft and Rockets*, 2015.

[38] Smith, D. L., Omidy, A. D., Weng, H., White, T. R., and Martin, A., "Effects of Water Presence on Low Temperature Phenomenon in PICA," *45th AIAA Thermophysics Conference*, AIAA Paper 2015-2664, Dallas, TX, June 22-26 2015, Accepted (Manuscript ID 2150042).

[39] Smith, D. L., White, T. R., and Martin, A., "Statistics on FIAT Conduction Modeling for MEDLI Arc Jet Testing," *45th AIAA Thermophysics Conference*, AIAA Paper 2015-2664, Dallas, TX, June 22-26 2015, Accepted (Manuscript ID 2149970).

[40] Martin, A. and Boyd, I. D., "Non-Darcian Behavior of Pyrolysis Gas in a Thermal Protection System," *Journal of Thermophysics and Heat Transfer*, January-March 2010.

[41] Mahzari, M., Braun, R. D., White, T., and Bose, D., "Preliminary Analysis of the Mars Science Laboratory's Entry Aerothermodynamic Environment and Thermal Protection System Performance," *AIAA 2013-0185*, January 2013.

[42] Beck, R. A. S., Driver, D. M., Wright, M. J., Laub, B., Hwang, H. H., Slimko, E. M., Edquist, K. T., Sepka, S. A., Willcockson, W. H., and Thames, T. D., "Development of the Mars Science Laboratory Heatshield Thermal Protection System," *41st AIAA Thermophysics Conference*, AIAA Paper 2009-4229, San Antonio, TX, 22 - 25 June 2009.

[43] Alkandry, H., Boyd, I. D., and Martin, A., "Comparison of Transport Properties Models for Flowfield Simulations of Ablative Heat Shields," *Journal of Thermophysics and Heat Transfer*, Vol. 28, No. 4, October 2014, pp. 569–582.

[44] Martin, A., Cozmuta, I., Boyd, I. D., and Wright, M. J., "Kinetic rates for gas phase chemistry of phenolic based carbon ablator decomposition in atmospheric air," *Journal of Thermophysics and Heat Transfer*, Vol. 29, No. 2, April 2015, pp. 222–240.

[45] Prabhu, D., Saunders, D., Tang, C., Terrazas-Salinas, I., Carballo, E., and Driver, D., "CFD Analysis Framework for Arc-Heated Flowfields, I: Stagnation

Testing in Arc-Jets at NASA ARC," *41st AIAA Thermophysics Conference*, AIAA Paper 2009-4080, San Antonio, TX, 22 - 25 June 2009 2009.

[46] Prabhu, D., Saunders, D., Tang, C., Terrazas-Salinas, I., Carballo, E., and Driver, D., "CFD Analysis Framework for Arc-Heated Flowfields, II: Shear Testing in Arc-jets at NASA ARC," *41st AIAA Thermophysics Conference*, AIAA Paper 2009-4081, San Antonio, TX, 22 - 25 June 2009 2009.

[47] White, T. R., Sepka, S. A., Beck, R. A. S., and Smith, D. M., "CFD and Material Response Framework for Wedge Testing in AEDC H2," *41st AIAA Thermophysics Conference*, AIAA Paper 2009-4233, San Antonio, TX, 22 - 25 June 2009.

[48] Milos, F. and Chen, Y.-K., "Ablation, Thermal Response, and Chemistry Program for Analysis of Thermal Protection Systems," *10th AIAA/ASME Joint Thermophysics and Heat Transfer Conference*, AIAA Paper 2010-4663, Chicago, IL, 28 June - 1 July 2010.

[49] Weng, H. and Martin, A., "Numerical Investigation of Thermal Response Using Orthotropic Charring Ablative Material," *Journal of Thermophysics and Heat Transfer*, Vol. 29, No. 3, July 2015.

[50] Tran, H. K., Johnson, C. E., Rasky, D. J., Hui, F., Hsu, M., Chen, T., Chen, Y., Paragas, D., and L.Kobayashi, "Phenolic Impregnated Carbon Ablators (PICA) as Thermal Protection Systems for Discovery Missions," Technical Memorandum 110440, NASA Ames Research Center, Moffett Field, CA, April 1997.

[51] Lachaud, J., Martin, A., Cozmuta, I., and Laub, B., "Ablation test-case series 1," *4th AFOSR/SNL/NASA Ablation Workshop*, 2010.

[52] Moyer, C. B. and Rindal, R. A., "An analysis of the coupled chemically reacting boundary layer and charring ablator. Part 2 - Finite Difference Solution for

the In-Depth Response of Charring Materials Considering Surface Chemical and Energy Balances," Contractor Report CR-1061, NASA, 1968.

[53] Haynes, W. M., editor, *CRC Handbook of Chemistry and Physics*, CRC Press, 95th ed., 2014.

Vita

David L. Smith

Education

- University of Kentucky, Lexington, KY

  Pursuing Master of Science in Mechanical Engineering, 2014-present

- University of Kentucky, Lexington, KY

  Bachelor of Science in Mechanical Engineering, Summa Cum Laude, 2014

  Bachelor of Science in Mathematics, Summa Cum Laude, 2014

Articles in Refereed Conference Proceedings

- Smith, D. L., White, T. R., and Martin, A., "Statistics on FIAT Conduction Modeling for MEDLI Arc Jet Testing," 45th AIAA Thermophysics Conference, AIAA Paper 2015-2664, Dallas, TX, June 22-26 2015, Accepted (Manuscript ID 2149970).

- Smith, D. L., Omidy, A. D., Weng, H., White, T. R., and Martin, A., "Effects of Water Presence on Low Temperature Phenomenon in PICA," 45th AIAA Thermophysics Conference, AIAA Paper 2015-2505, Dallas, TX, June 22-26 2015, Accepted (Manuscript ID 2150042).